Design of Dielectric Resonator Antenna Arrays for High Speed Short Range MIMO Communications

BY

Mohamed Tammam Hussein

A Thesis Presented to the
DEANSHIP OF GRADUATE STUDIES

KING FAHD UNIVERSITY OF PETROLEUM & MINERALS
DHAHRAN, SAUDI ARABIA

In Partial Fulfillment of the
Requirements for the Degree of

MASTER OF SCIENCE

In

Electrical Engineering

May 2016

KING FAHD UNIVERSITY OF PETROLEUM AND MINIRALS

DHAHRAN 31261, SAUDI ARABIA

DEANSHIP OF GRADUATE STUDIES

This thesis, written by **Mohamed Tammam Hussein** under the direction of his thesis advisor and approved by his thesis committee, has been presented to and accepted by the Dean of Graduate Studies in partial fulfillment of the requirements for the degree of **MASTER OF SCIENCE IN ELECTRICAL ENGINEERING.**

Dr. Mohammad Sharawi
(Advisor)

Dr. Ali Al-Shaikhi
Department Chairman

H. Masoudi 25-5-2016

Dr. Husain Masoudi
(Member)

Dr. Salam A. Zummo
Dean of Graduate Studies

Dr. Essam Hassan
(Member)

31/5/16

Date

To my fiancée

To my parents

ACKNOWLEDGMENTS

At first, I would like to thank AMSDL group members who inspired my thinking and enhanced my knowledge during the weekly group sessions. Special thanks to Dr. Umar Khan, Dr. Rifaqat Hussain and Mr. Ali Al-Reshaid who helped in some parts of my work. Many appreciations to Dr. Symon Podilchak and Dr. Yahia Antar from the Royal Military college in Canada who contributed to this work especially in the fabrication part. I would like also to thank the committee members, Dr. Husain Masoudi and Dr. Essam Hassan for their valuable comments and suggestion throughout this work. It goes without saying, all my gratitude to my advisor Dr. Mohammad Sharawi who was not only there in every step of this work but also supported me on both the academic and personal levels.

I would like to thank my colleagues and my manager in Rawabi United Safety Services – Engineering, Research and Development group as well as the management of Rawabi Holding who made it easier to continue my higher studies while depending on me in my daily work. Many thanks to Mr. Mohammed Shahin who intervened in the right time to assure my continuation of the master degree. More importantly, I would like to thank my parents whose support and prayers made it even easier throughout the years.

Special warm and heartfelt thanks to my fiancée, Reina. It would not have been possible to do any of any of this without you on my side. You are constantly making me pursuing the best paths in everything. Thank you very much.

TABLE OF CONTENTS

LIST OF TABLES

LIST OF FIGURES

LIST OF ABBREVIATIONS

5G	:	Fifth Generation
cDRA	:	cylindrical Dielectric Resonator Antenna
DRA	:	Dielectric Resonator Antenna
ECC	:	Envelop Correlation Coefficient.
GHz	:	Giga-hertz
IoT	:	Internet of Things
LTE	:	Long Term Evolution
MHz	:	Mega-hertz
MIMO	:	Multiple-Input-Multiple-Output
mm-waves	:	millimeter waves

THESIS ABSTRACT

Full Name:	Mohamed Tammam Hussein
Title of Study:	Design of Dielectric Resonator Antenna Arrays for High Speed Short Range MIMO Communications.
Major Field:	Electrical Engineering
Date of Degree:	May 2016

Multiple-input-multiple-output (MIMO) technology is a vital solution for enhancing channel capacity for the upcoming 5G standard. With high benchmarks in terms of data rates, range and latency set for 5G future devices, utilizing the millimeter-wave (mm-wave) spectrum to provide the high bandwidth required is evident. Designing MIMO antenna systems is challenging due to the inter-related parameters that need to be considered in the design. However, in the mm-wave range, the disadvantage of the large size of MIMO antenna systems becomes negligible. Dielectric Resonators Antennas (DRA) are known to provide high-gain, high-efficient antenna elements due to the absence of metallic losses which makes them a viable solution to design mm-wave antenna systems.

In this work, two configurations for mm-wave DRA-based MIMO antenna systems were investigated; a 2-port and a 4-port MIMO systems with DRA based elements. Each port of the MIMO antenna system consists of a linear array of 4 DRA elements. Each DRA is a cylindrical type one that resonates at 30 GHz and provides a bandwidth of at least 1

GHz. The linear array of the cylindrical DRAs (cDRAs) has a dedicated feed network with tuned progressive phases to provide beam tilting and yields a good MIMO performance via the low values of correlation coefficient obtained. A Single 4-element array occupies 20 x 3.2 x 3.1 mm^3 *while its feed network occupies 20 x 12 mm*^{2}*. The 2-port configuration was fabricated to validate the design. Some discrepancies were found between measurement and simulation reflection coefficient response for which a thorough analysis was conducted. DRA misplacement due to human as well as DRA diameter errors due to manufacturing were found to be the major contributors. Clear tilts towards the desired direction for each array were observed. A gain of 8 dBi was achieved in both simulations and measurement with radiation efficiency higher than 90%. This makes such designs suitable for handheld portable devices.*

ملخص الرسالة

الاسم الكامل: محمد تمام أمين همام حسين

عنوان الرسالة: تصميم هوائيات عازلة الرنين لأنظمة متعددة المدخلات ومتعددة المخرجات قصيرة المدي عالية السرعة

التخصص: الهندسة الكهربائية

تاريخ الدرجة العلمية: مايو 2016

تعد تكنولوجيا متعددة المدخلات ومتعددة المخرجات (MIMO) حلا حيويا لتعزيزمدى استيعاب القنوات اللاسلكية الضرورية لتكنولوجيا الجيل المقبل من الاتصالات الجيل الخامس 5G. إنه من البديهي استخدام الترددات ذات الطول الموجي الميلليمتري في أجهزة 5G المستقبلية نظرا لما توفره هذه الموجات من نطاق عريض. إن تصميم النظم الهوائية متعددة المدخلات ومتعددة المخرجات (MIMO) يمثل تحديا بسبب العوامل المترابطة التي تحتاج إلى النظر عند التصميم جدير بالذكر أنه الترددات ذات الطول الموجي الميلليمتري يصبح العيب من الحجم الكبير من أنظمة الهوائي (MIMO) لا يكاد يذكر. ومن المعروف أن هوائيات عازل الرنين (DRA) توفر مكاسب عالية؛ فهي عناصرتذبذبية عالية الكفاءة بسبب عدم وجود خسائر المعدنية مما يجعلها حلا فعالا لتصميم أنظمة الهوائيات في ترددات ذات الطول الموجي الميلليمتري.

في هذا العمل، وقد تم تصميم اثنين من نماذج لأنظمة الهوائي (MIMO) القائم على (DRA) و استخدام ترددات ذات الطول الموجي الميلليمتري وهي نظام (MIMO) بمنفذين و نظام بأربعة منافذ معتمدين على(DRA). كل منفذ من النظام الهوائي (MIMO) يتكون من مجموعة خطية من 4 عناصر(DRA) . كل (DRA) هو من نوع أسطواني يتردد صداه في 30 غيغاهرتز، ويوفر عرض نطاق ترددي لا يقل عن 1 جيجاهرتز.كل مجموعة خطية من (DRA) أسطواني (cDRAs) لديها شبكة تغذية مخصصة لتوفير شعاع مائل بزاوية مدروسة مما يترتب عليه أداء (MIMO)

جيد من خلال القيم المنخفضة من معامل الارتباط التي تم الحصول عليها. كل مجموعة واحدة من 4-عناصر هوائية تحتل مساحة 20 × 3.2 × 3.1 مم مكعب في حين تحتل شبكة امداداتها 20 × 12 مم مربع .كما تم تصنيع النموذج ذي المنفذين للتحقق من صحة التصميم. تم العثور على بعض التناقضات بين القياس و المحاكاة من حيث استجابة معامل انعكاس واللذي من أجله أجري تحليلا دقيقا. حيث وجد بعض الأخطاء البشرية في تثبيت (DRA) في موضعها، فضلا عن الأخطاء التصنيعية لقطر (DRA) ليكونا المساهمين الرئيسيين في التناقضات. لقد حقق التصميم معامل تضخم بلغت 8 ديسيبل في كل من المحاكاة والقياس مع كفاءة إشعاع أعلى من 90٪. وهذا ما يجعل هذه التصاميم مناسبة للأجهزة المستقبلية المحمولة باليد.

CHAPTER 1

INTRODUCTION

In this chapter, recent advances in communications, future communication standards and requirements are discussed. An introduction on Dielectric Resonator Antennas (DRAs) and its history as well as the arising technology of Multiple-Input-Multiple-Output (MIMO) systems are presented. Finally, the motivation behind this work and its objectives are stated.

1.1 5G Wireless Standard: The Future for High Speed Short Range Communications

As the Long Term Evolution (LTE) and 4G technology are reaching their limits in terms of data rates and spectrum use, a new generation for mobile communications is emerging which is denoted as 5G. Figure 1.1 shows the evolution of the communication standards and corresponding applications. While current and previous generations were limited in terms of applications to user devices, 5G will connect almost everything. Millimeter waves (mm-waves) (28.5 GHz – 100 GHz) are the potential resource for the upcoming generation due to its ability to provide higher bandwidth –and hence- higher data rates. Data rates of 5 Gbps, compared to a maximum of 100 Mbps for LTE networks, are targeted to be achieved. The key for achieving this high data rate is to utilize higher bandwidth that is available in the mm-wave ranges but at the expense of the shorter covered range [1].

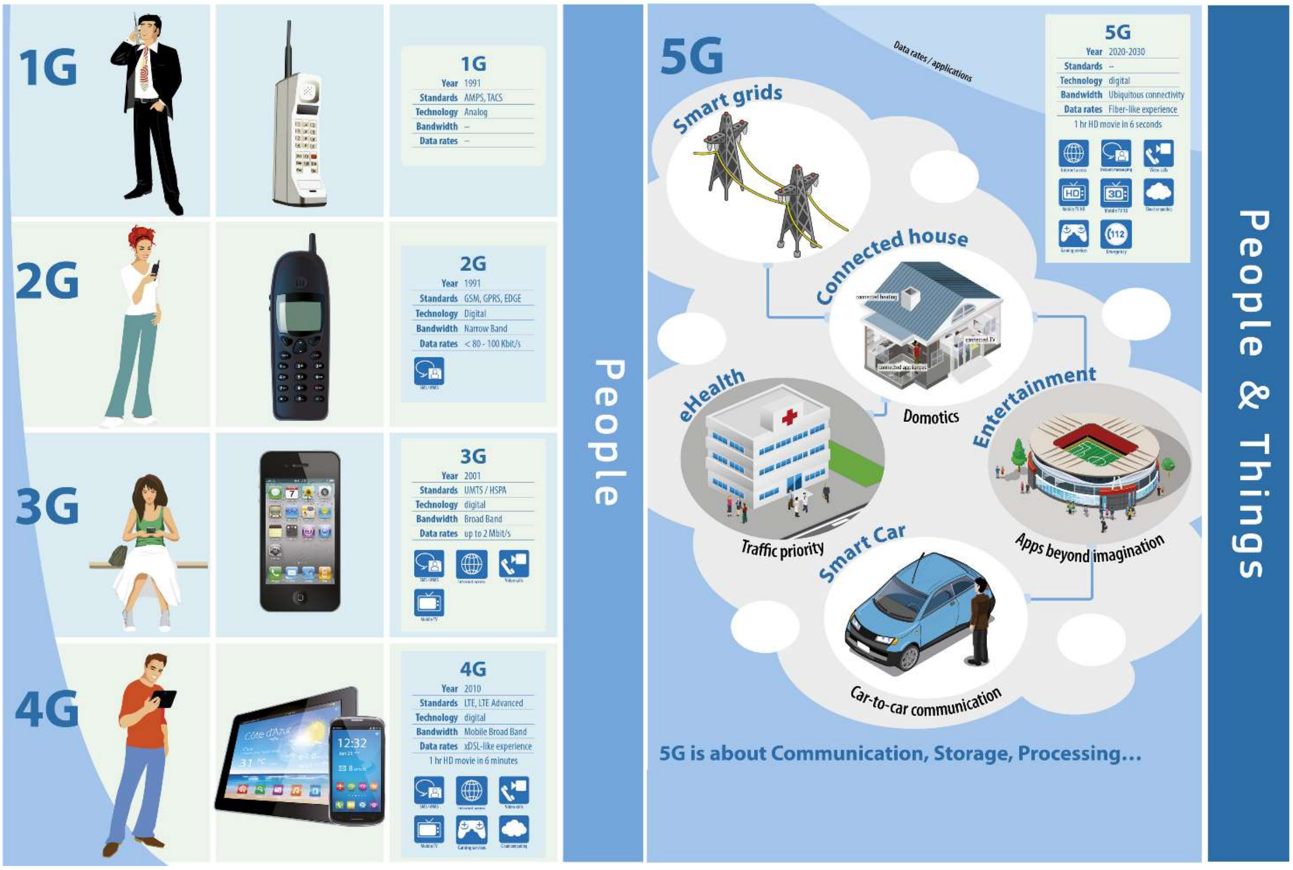

Figure 1.1:Evolution of wireless standards [1]

Many recent attempts intended to characterize or define the standard for 5G. The most recent was the IEEE 5G Summit held on May 26th, 2015. The summit focused on the enabling technologies for 5G. These technologies include: Internet of Things (IoT), MIMO and massive MIMO, mm-Wave as well as other technologies related to networking and embedded systems as shown in Figure 1.2. Target objectives of the upcoming standard 5G are higher network capacity with lower latency, accommodation for large number of devices for IoT applications, forming Ad-Hoc networks for industrial and vehicular applications while maintaining robustness for critical applications.

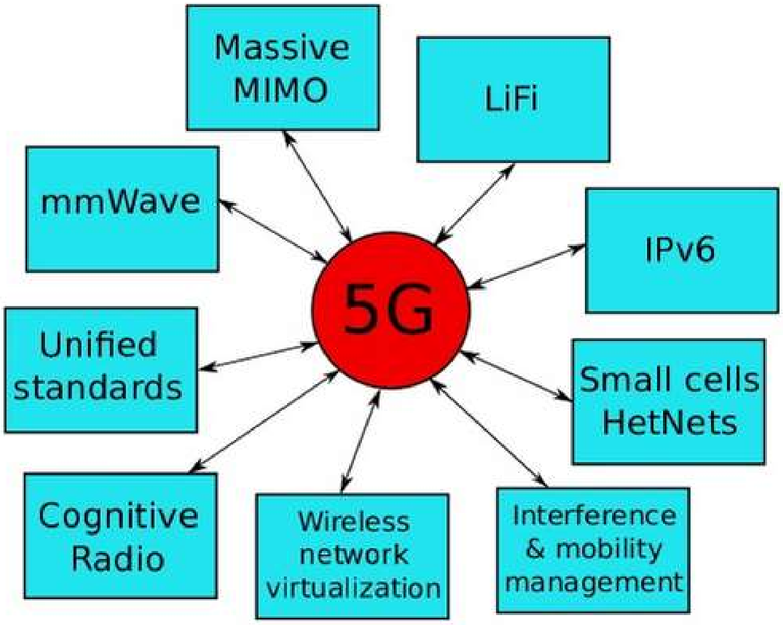

Figure 1.2: 5G enabling technologies [2]

1.2 Multiple-Input-Multiple-Output (MIMO) Systems

The need for MIMO systems arose from the need of achieving higher data throughput and reliability for the wireless communication systems using limited power levels and frequency bandwidth. Different configurations were adopted by wireless systems to enhance system throughput and diversity [3]. For example, in single-input-multiple-output (SIMO) systems, the transmitter has one antenna while the receiver has multiple antennas. On the other hand, in a multiple-input-single-output (MISO) system, the transmitted signal is coded uniquely multiple times and transmitted over multiple antennas.

One receiver with one antenna will receive the uniquely coded signals and decode them. Both configurations (SIMO and MISO) provide performance enhancement in terms of resistance to fading and power management.

MIMO utilizes beamforming, spatial multiplexing and diversity coding together or independently. With knowledge of the channel state, multiple streams at the same frequency are transmitted simultaneously through multiple antennas and received by multiple antennas. At the receiver, MIMO algorithms are used to decode the signal utilizing antenna diversity to provide higher data rates. This can be explained by the increase in channel capacity according to the simplified ideal scenario of a real multipath environment in (1) where N represents the number of MIMO antenna ports and B is the available bandwidth. It can be seen from (1) that the channel capacity (C) is directly proportional to N under the same SNR and Bandwidth. However, the disadvantages of MIMO are the increase in computational cost and the additional hardware which means higher cost and larger size [3].

$$C = NB\log_2(1 + SNR) \tag{1.1}$$

The challenge in designing MIMO antennas is to assure providing the MIMO system with the required spatial diversity such that equation (1.1) will be applicable. This is done by designing the MIMO antenna system with low correlation coefficient between all MIMO elements [4]. Other factors to be taken into consideration are similar to those in any antenna design such that: Gain (total gain), efficiency, operating bandwidth and radiation pattern.

1.3 Dielectric Resonator Antennas (DRAs)

Dielectric Resonators (DRs) were firstly introduced by Richtinger in 1939. The modes of the DRs were theoretically analyzed and studied by Okaya and Barash in the 1960s. Since then, DRs were used in microwave circuits as high Q elements (low loss) to realize circuit devices such as filters and oscillators exceeding the existing waveguide cavity technology in terms of compactness and manufacturability as printed circuit elements. That was motivated by the development of ceramic materials of low loss tangent in the 1960s. For such applications, DRs were usually shielded by metal cavities to preserve the energy within them [5].

DRs were first proposed as radiating elements denoted as DR antennas (DRAs) by Long, McAllister and Shen in the early 1980s. Basic shapes including Hemispherical, Cylindrical, and Rectangular DRAs were studied covering their resonant modes, radiation patterns and excitation methods. Extensive research was conducted by two research groups led by Kishk, Glisson and Junker as the first group and Luk and Leung as the second group [5]. A comprehensive review of the earlier work on DRA analysis and design was presented in 1994 by Mongia and Bhartia [6].

DRAs offer many advantages over printed circuit metallic antennas. The common ones are:

1. Highly efficient radiation due to absence of surface waves and conductor (Ohmic) losses which become a major issue in mm-wave ranges.
2. Design flexibility hence the resonance frequency and Q-factor (BW) are affected by the aspect ratio for a DRA of a certain dielectric permittivity

3. Variety of resonance modes can be excited from the same geometry allowing for wide band and multiple band applications
4. The ability to be excited by almost all conventional printed circuit feeding methods such as microstrip or slot feed with advantages and disadvantages for each [7].

However, DRAs have a couple of disadvantages including:

1. Higher machining and assembly cost compared to printed antenna.
2. Their 3D structure might not make them suitable for small installations where a superstrate or a cavity is very close above the antenna system.

Since their introduction, several DRA based designs were proposed for various wireless communication applications as will be discussed in Chapter 3.

1.4 Work Motivation

Higher throughput, higher speed links, dense network and seamless connectivity of everything are the driving forces behind the continuous development in communication technologies and standards. Efficient utilization of the spectrum and the channel is advantageous in any design. Hence, a compact MIMO antenna system operating in the upcoming 5G frequency range is a promising solution. MIMO is an enabling technology to be used in the future 5G systems due its many advantages such as increasing channel capacity and overcoming the effects of channel fading. However, the design of MIMO systems –and antennas- is challenging. Many parameters that are not always independent need to be taken into consideration.

For the mm-wave spectrum (30GHz-300 GHz) conventional metallic antennas are not efficient due to conductor losses and surface waves which are directly proportional to frequency. Also, when combined with MIMO, high coupling because of the surface waves is always of an issue. Hence, the use of DRAs is proposed as a potential candidate for these antennas operating at high frequencies since no conductor losses exist. The only disadvantage of the DRAs is introducing the third dimension. However, this can be neglected since the overall size of a DRA resonating at mm-wave is very small (less than 5x5x5 mm^3) as will be shown in the coming sections.

1.5 Thesis Objectives

The objectives of this work are:

1. To design a cDRA antenna resonating at 30 GHz and having 1 GHz minimum bandwidth.
2. To design a linear array of 4 cDRAs along with its feed network with predefined progressive phases to allow for radiation pattern beam tilting.
3. To design and simulate a MIMO antenna system utilizing the linear array and assess the system performance.
4. To fabricate the optimized design and correlate measurements with simulated results.

CHAPTER 2

BACKGROUND

A brief background is presented in this section. The background will introduce the basic antenna parameters, then it will cover the DRA definition, theory of operation and design formulas and –finally- will discuss important MIMO antenna metrics.

2.1 Basic Antenna Parameters

An antenna is defined as "*structures for emitting and/or receiving radio waves*" [8]. In other words, the antenna is the medium that converts guided electromagnetic waves from the system into radiated waves in the air –or transmission medium- and vice versa. Antenna design has evolved over the years resulting in a number of designs and technologies. In the literature, Antennas that are fed by printed circuit technology dragged great attention due to their low profile, low cost and ability to integrate them with printed circuit board technology. In general, the parameters that need to be analyzed of any antenna are:

2.1.1 Resonating Frequency

The Thevenin equivalent model of an antenna is shown in Figure 2.1 [8]. The resonance of the antenna occurs when the reactive part of the input impendence is zero. A single antenna can have one resonance frequency resulting in single band operation while other antennas can have two or more resonating frequencies resulting in dual or multi-band operation. However, the challenge to the latter –among others- is matching the input impendence of the antenna to the feeding mechanism. The resonance frequency of the antenna is inversely propositional to its size.

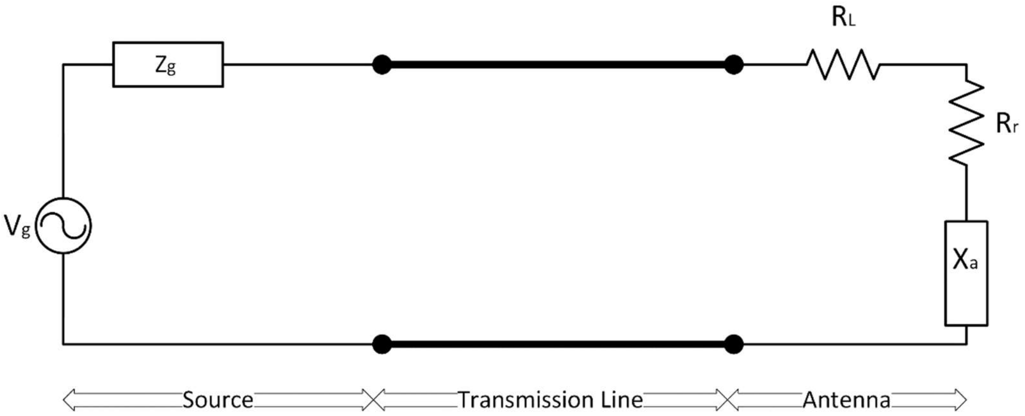

Figure 2.1 Antenna Thevenin equivalent

2.1.2 Frequency Bandwidth

The frequency bandwidth (BW) of an antenna can be defined as the difference between frequency points that corresponds to -10 dB on its reflection coefficient curve. In some cases, -6 dB points are considered for miniaturized and wide band antennas to relax matching the requirements. The BW can be expressed in terms of the fractional bandwidth according to (2.1) where f_2 is the higher frequency point, f_1 is the lower frequency point and f_c is the center frequency. The fractional bandwidth is the reciprocal of the antenna Q-factor according to (2.2).

$$FBW = \frac{f_2 - f_1}{f_c} \tag{2.1}$$

$$Q = \frac{1}{FBW} = \frac{f_c}{f_2 - f_1} \tag{2.2}$$

2.1.3 Radiation Pattern

The radiation pattern is a 2D or 3D spatial representation of the electric field –or the energy- radiated from the antenna in the far field which also can be modeled as mathematical equation relating the field strength and the space coordinates [8].

2.1.4 Efficiency

The efficiency of a system is defined as the ratio of the output with respect to the input. In antennas, the efficiency of an antenna system is the ratio of radiated power from the antenna to the input power to the antenna system. For printed antennas, the efficiency is controlled by three factors: conductor losses, impendence mismatch losses and dielectric losses. Equation (2.3) gives the total efficiency e_0 of the antenna in terms of conductor efficiency e_c, dielectric efficiency e_d and mismatch efficiency e_r [8].

$$e_0 = e_c e_d e_r \tag{2.3}$$

2.1.5 Directivity

An isotropic antenna is theoretical point of radiation that radiates power equally in all directions. However, this antenna cannot be practically realized. Omni directional antennas radiates power equally in one plane (vertical or horizontal cross section). Other antennas are directional i.e. they radiate power in a certain direction more than other. Directivity is the ratio of the radiation intensity in a certain direction to the total radiated power [8] as shown in (2.4). The maximum gain of the antenna is found at its direction (maximum directivity location).

$$D(\theta,\emptyset) = \frac{U(\theta,\emptyset)}{P_{rad}/_{4\pi}} = \frac{4\pi\, U(\theta,\emptyset)}{P_{rad}} \qquad (2.4)$$

2.1.6 Gain

The gain is a dimensionless quantity and one can define it as the maximum power radiated from the antenna in the direction of the antenna with respect to the input power. The gain is therefore expressed in terms of directivity and efficiency in equation (2.5).

$$G(\theta,\emptyset) = e_0\, D(\theta,\emptyset) \qquad (2.5)$$

2.2 Dielectric Antenna Resonators (DRAs): Theory and Design

This section gives a brief introduction about the DRAs and then it will focus on the cylindrical DRA (cDRA) theory and design.

2.2.1 DRA definition, shapes, and features

A Dielectric Resonator Antenna (DRA) consists of a dielectric material of a certain shape and dimensions with a dielectric constant of ε_r. The structure is usually fixed on a large ground plane with infinite conductivity [5]. The DRA can be of any shape as depicted in Figure 2.2. However, basic shapes that are studied extensively in the literature include hemispherical, cylindrical and rectangular shapes [7]. Other shapes were also investigated such as low profile disks, annular and triangular DRAs. Some modifications such as introducing gaps and slits are used to modify the behavior of the DRA such as increasing the bandwidth or obtain circular polarization radiation, etc.

Figure 2.2 Various DRA Shapes [7]

DRAs have many advantages over the conventional metallic printed antennas. These advantages include [5]:

- DRA Size

  The size of the DRA is directly proportional to $\lambda_0/\sqrt{\varepsilon_r}$ where λ_0 is the free space wavelength and ε_r is the dielectric constant of the antenna. Hence, the designer has the flexibility to control the size by changing/choosing the material from a wide range of dielectric constants (10-100) at the expense of its bandwidth. The higher the ε_r, the lower the bandwidth (higher Q-factor).

- Resonance Frequency and Bandwidth

  In addition to ε_r, the resonance frequency and bandwidth are affected by the aspect ratio of the antenna which – in case of a cylindrical DRA- is ratio of the radius of its base to the height of the antenna or (a/h).

- High Efficiency

  Since the surface waves and metallic losses are not present in dielectric resonators along with low loss tangent values, the total efficiency of the DRAs are very high as expected from equation (2.3). This is very advantageous in mm-wave applications where metallic losses are dominant.

- Design Flexibility

  Since DRAs are 3D structures, they offer additional degrees of freedom that allow the designer to control some design parameters. For example, in cDRAs, the designer can choose between different heights for the same aspect ratio giving him/her flexibility over the bandwidth.

- Integration with printed circuit technology

  DRAs can be excited by almost all microstrip feeding mechanisms including direct feed, aperture coupling, probe…etc. Each mechanism will excite certain modes of the DRA and has its advantages and disadvantages. Design requirement and constrains sometimes forces the designer to choose one mechanism or another.

2.2.2 cDRA Design

Many attempts in the literature took place to set guidelines for designing a cDRA. Two sources [5] - [6] provided comprehensive set of equations and curves for the resonance frequency and Q-factor findings based on the material type and shape. These equations do not take into account the effect of the feed and assume that the cDRA is fixed on top of a large ground plane with infinite conductivity.

The center frequency of a cDRA can be calculated using:

$$f(GHz) = \frac{30k_o a}{2\pi h(a/h)} \tag{2.6}$$

where k_o is the free space wave number, h is the height of the cDRA in cm, a/h is the aspect ratio of the cDRA and h=2d as shown in Figure 2.3. The $k_o a$ is calculated as one quantity from the design equations listed in Table 1 and hence “a” will not cancel out from the numerator and denominator.

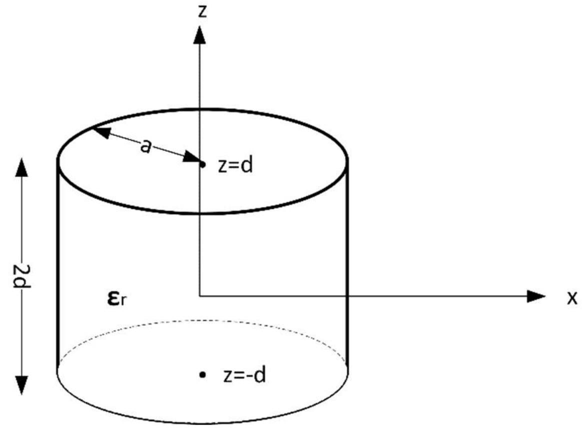

Figure 2.3: Geometry of a cDRA

As pointed out in 2.2.1, the frequency and the bandwidth are affected by the dimensions of the cDRA and its dielectric constant. Table 1 shows the first five fundamental modes excited inside the cDRA and their corresponding equations for $k_o a$ and Q-factor. These modes are usually targeted when designing the antennas. Higher modes are more difficult to excite and hence to radiate. The frequency and bandwidth can be calculated from these quantities as shown in (2.2) and (2.6).

Table 1: cDRA fundamentals modes and design equation summaries

Mode	Equation	Criteria
$\mathbf{TE_{01\delta}}$	$k_o a = \frac{2.327}{\sqrt{\varepsilon_r+1}}\{1 + 0.2123\frac{a}{h} - 0.00898(\frac{a}{h})^2\}$ (2.7)	

	$Q = 0.078192\varepsilon_r^{1.27}\{1 + 17.31\left(\frac{h}{a}\right) - 21.57\left(\frac{h}{a}\right)^2 + 10.86\left(\frac{h}{a}\right)^3 - 1.98(\frac{h}{a})^4\}$ (2.8)	$0.5 \leq \left(\frac{a}{h}\right) \leq 5.0$
$\mathbf{TM_{01\delta}}$	$k_o a = \sqrt{\frac{3.83^2 + (\frac{\pi a}{2h})^2}{\varepsilon_r + 2}}$ (2.9)	$0.33 \leq \left(\frac{a}{h}\right) \leq 5.0$
	$Q = 0.00872\varepsilon_r^{0.888413}e^{0.039747\varepsilon_r}\left\{1 - \left(0.3 - 0.2\left(\frac{a}{h}\right)\right)\left(\frac{38-\varepsilon_r}{28}\right)\right\}\left\{9.498186\left(\frac{a}{h}\right) + 2058.33\left(\frac{a}{h}\right)^{4.322261} e^{-3.50099\left(\frac{a}{h}\right)}\right\}$ (2.10)	
$\mathbf{HE_{11\delta}}$	$k_o a = \frac{6.324}{\sqrt{\varepsilon_r + 2}}\left\{0.27 + 0.36\frac{a}{2h} + 0.02\left(\frac{a}{2h}\right)^2\right\}$ (2.11)	$0.4 \leq \left(\frac{a}{h}\right) \leq 6.0$
	$Q = 0.01007\varepsilon_r^{1.3}\frac{a}{h}\left\{1 + 100e^{-2.05\left(\frac{a}{2h} - \frac{1}{80}\left(\frac{a}{h}\right)^2\right)}\right\}$ (2.12)	
$\mathbf{TE_{011+\delta}}$	$k_o a = \frac{2.208}{\sqrt{\varepsilon_r + 1}}\left\{1.0 + 0.7013\left(\frac{a}{h}\right) - 0.002713\left(\frac{a}{h}\right)^2\right\}$ (2.13)	$0.5 \leq \left(\frac{a}{h}\right) \leq 5.0$
	$Q = 0.03628\varepsilon_r^{2.38}\left\{-1.0 + 7.81\left(\frac{a}{h}\right) - 5.858\left(\frac{a}{h}\right)^2 + 1.277\left(\frac{a}{h}\right)^3\right\}$ (2.14)	
$\mathbf{HE_{12\delta}}$	$k_o a = \frac{3.72 + 0.4464\left(\frac{a}{2h}\right) + 0.2232\left(\frac{a}{2h}\right)^2 + 0.0521\left(\frac{a}{2h}\right)^3 - 2.65e^{-1.25\left(\frac{a}{2h}\right)(1+4.7\left(\frac{a}{2h}\right))}}{\sqrt{\varepsilon_r}}$ (2.15)	

	$Q=\varepsilon_r{}^2\left\{0.068-0.0388\left(\frac{a}{2h}\right)+0.0064\left(\frac{a}{2h}\right)^2+0.0007e^{\left(\frac{a}{2h}\right)\left(37.59-63.8\left(\frac{a}{2h}\right)\right)}\right\}$ (2.16)	$0.5 \le \left(\frac{a}{h}\right) \le 5.0$

The subscripts represent to the variations of the fields in azimuth (Φ), radial (r) and axial (z) directions respectively. δ is a number that varies between 0 and 1 and approaches 1 for high values of ε_r. It must be noted that the design equations in Table 1 are approximations based on field equations with many assumptions for the boundary conditions [7]. Also, they do not account for loading effects by the feed or consider limited size of ground planes [5]. To incorporate all the effects in a practical design, the above equations are used a starting point and then the design is optimized and finalized using a Full wave solver.

2.2.3 cDRA Design Procedure

To design a cDRA, one should have four input design parameters: center frequency bandwidth, desired resonating mode and the dielectric constant(s) of available material(s). The procedure for the design follow the following steps [5]:

1. Start with an estimation for a and h. Take into account the criteria for the aspect ratio for the selected mode.
2. Calculate the quantities $k_o a$ and Q from equations (2.7)-(2.16) based on the mode to be excited.
3. Calculate the center frequency and the bandwidth from (2.2) and (2.6).

4. If the obtained frequency is less/more than the target frequency, decrease/increase the aspect ratio and repeat 2 and 3.
5. If the obtained bandwidth is less/more than the target bandwidth, decrease/increase the aspect ratio and repeat 2 and 3.

2.2.4 Fields inside the cDRA

Circular waveguide and cavity approach can be used to find the resonant modes and field equations inside the cDRA [9]. The lowest mode that can be realized for a cylindrical dielectric resonator is $TE_{01\delta}$ which corresponds to TE_{011} in a metallic circular cavity. The subscripts refer to the variations of the fields in azimuth (Φ), radial (r) and axial (z) directions respectively. The symbol δ represents a value from 0 to 1 and approaches 1 for high values of ε_r. Unlike a metallic cavity, the fields do not vanish at the walls of the cavity, instead –for a dielectric resonator, the fields penetrates the surfaces but fades in the air (evanescent fields) as shown in Figure 2.4 where it shows $\delta = \mathrm{L}/\lambda_g$ where λg is the guided wavelength inside the resonator and L is the height of the dielectric resonator where L =2d.

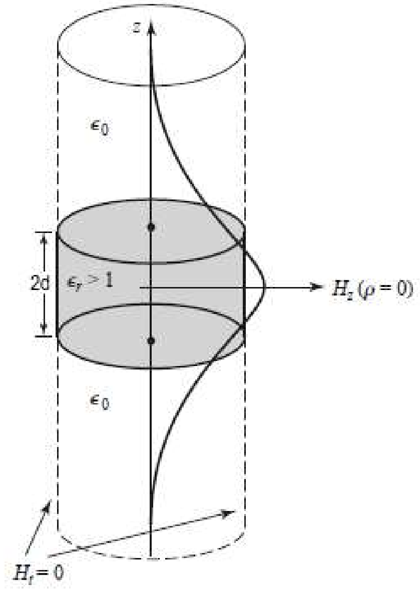

Figure 2.4: H_z Field inside DRA for $TE_{01\delta}$ [9]

From circular waveguide theory [9], the set of transverse field equations in cylindrical coordinates for a circular waveguide are:

$$E_\rho = \frac{-j}{k_c^2}\left(\beta\frac{\partial E_z}{\partial\rho} + \frac{\omega\mu}{\rho}\frac{\partial H_z}{\partial\phi}\right) \tag{2.17}$$

$$E_\phi = \frac{-j}{k_c^2}\left(\frac{\beta}{\rho}\frac{\partial E_z}{\partial\phi} - \omega\mu\frac{\partial H_z}{\partial\rho}\right) \tag{2.18}$$

$$H_\rho = \frac{j}{k_c^2}\left(\frac{\omega\epsilon}{\rho}\frac{\partial E_z}{\partial\phi} - \beta\frac{\partial H_z}{\partial\rho}\right) \tag{2.19}$$

$$H_\phi = \frac{-j}{k_c^2}\left(\omega\epsilon\frac{\partial E_z}{\partial\rho} - \frac{\beta}{\rho}\frac{\partial H_z}{\partial\phi}\right) \tag{2.20}$$

where E is the electric field intensity (V/m), H is the magnetic field intensity (A/m), ω is the angular frequency, ϵ and μ are the permittivity and the permeability of the material inside the waveguide respectively, β is the propagation constant and $k_c^2 = k^2 - \beta^2$.

For TE modes where there is no electrical field component in the direction of the wave propagation (E_z=0), the wave equation is given by:

$$\nabla^2 H_z + k^2 H_z = 0 \tag{2.21}$$

Where k=$\sqrt{\varepsilon_r}$ k_o for |z|<L/2 , and k=k_o for |z|> L/2. The solution to the wave equation (22) is given in (2.22) where J_0 is Bessel function of the first kind.

$$H_z = H_0 J_0(k_c \rho) e^{\pm j\beta z} \tag{2.22}$$

Since there is no change in the fields in the azimuth direction for the first mode and a magnetic wall condition ($H_{tangential}$=0) is applied at ρ=a. Equations (2.17) -(2.20) reduce to:

$$E_\phi = \frac{j\omega\mu}{k_c^2} \frac{\partial H_z}{\partial \rho} \tag{2.23}$$

$$H_\rho = \frac{-j\,\beta}{k_c^2} \frac{\partial H_z}{\partial \rho} \tag{2.24}$$

Assuming a magnetic wall condition ($H_{tangential}$=0) at ρ=a, we can write the field equations of the first mode TE_{01} for the dielectric waveguide as follows [9]:

$$E_\phi = \frac{j\omega\mu}{k_c^2} H_0 J_0'(k_c \rho) e^{\pm j\beta z} \tag{2.25}$$

$$H_\rho = \frac{\pm j\,\beta}{k_c^2} H_0 J_0'(k_c \rho) e^{\pm j\beta z} \tag{2.26}$$

The propagation constant will be real inside the DR (stored) while it will be imaginary in the air (propagating or evanescent). We can write:

$$\alpha = \sqrt{k_c^2 - k_0^2} = \sqrt{\left(\frac{p_{01}}{a}\right)^2 - k_0^2} \tag{2.27}$$

$$\beta = \sqrt{\varepsilon_r k_0^2 - k_c^2} = \sqrt{\varepsilon_r k_0^2 - \left(\frac{p_{01}}{a}\right)^2} \tag{2.28}$$

Where p_{01} is the first root of the derivative of the first Bessel function. The wave impedance is the ratio of the electric field to the magnetic field. So we can write:

$$Z_d = \frac{E_\phi}{H_\rho} = \frac{\omega\mu}{\beta} \tag{2.29}$$

$$Z_a = \frac{E_\phi}{H_\rho} = \frac{j\omega\mu}{\alpha} \tag{2.30}$$

Where the subscripts ‘d’ and ‘a’ refers to the dielectric and air respectively.

To find the resonance frequency for the first mode –which is even around z- we can rewrite (2.25)-(2.26) using (2.27) - (2.30) as follows:

$$\text{inside the DR} \begin{cases} E_\phi = A J_0'(k_c\rho)\cos\beta z \\ H_\rho = \frac{-j\,A}{Z_d} J_0'(k_c\rho)\sin\beta z \end{cases} \tag{2.31}$$

$$\text{in the air} \quad \begin{cases} E_\phi = B J_0'(k_c\rho) e^{-j\alpha|z|} \\ H_\rho = \frac{\pm j\,B}{Z_a} J_0'(k_c\rho) e^{-j\alpha|z|} \end{cases} \tag{2.32}$$

Using boundary conditions at z=L/2 for the electric and magnetic fields:

$$E_\phi\left(\frac{\text{L}}{2}\right)\text{inside the DR} = E_\phi\left(\frac{\text{L}}{2}\right)\text{in the air} \tag{2.33}$$

$$B_\rho\left(\frac{\text{L}}{2}\right)\text{inside the DR} = B_\rho\left(\frac{\text{L}}{2}\right)\text{in the air} \tag{2.34}$$

And since the two materials are dielectric (relative permeability=1), we can reduce equations (32) and (33) to:

$$-jZ_a \sin\beta\frac{L}{2} = Z_d \cos\beta\frac{L}{2} \tag{2.35}$$

which can be reduced using (30) and (31) to

$$\tan\beta\frac{L}{2} = j\frac{Z_d}{Z_a} = \frac{\alpha}{\beta} \tag{2.36}$$

As noted from (2.36), the resonance frequency can be found numerically since the equation contains k_0 if the dimensions of the cylindrical DR (a and L) and its dielectric constant are known.

2.2.5 Coupling to cDRAs

The key to excite a cDRA with a certain desired mode –assuming the cDRA geometry is designed to resonate at that mode- is by using an equivalent field source and place it where the corresponding strongest field lines reside the DRA. For example, to excite $TM_{01\delta}$ mode, a probe (an electric current source) is placed at the center of the cDRA where a strong electric field exists as shown in Figure 2.5 [5].

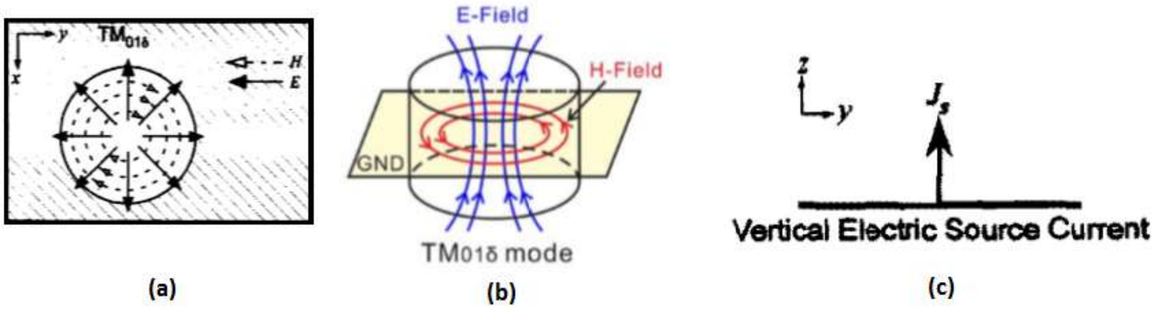

Figure 2.5: electric and magnetic fields inside the cDRA for $TM_{01\delta}$ mode (a) top view [5]. (b) 3D view [10]. (c) Electric source equivalent for a vertical probe [5]

To excite the $TE_{01\delta}$ mode, aperture coupling is usually used. The aperture (or slot) can be modeled as a magnetic source equivalent. As shown in Figure 2.6, a strong magnetic field exists at the bottom side of the cDRA at its center which makes it a good location to place the slot [5].

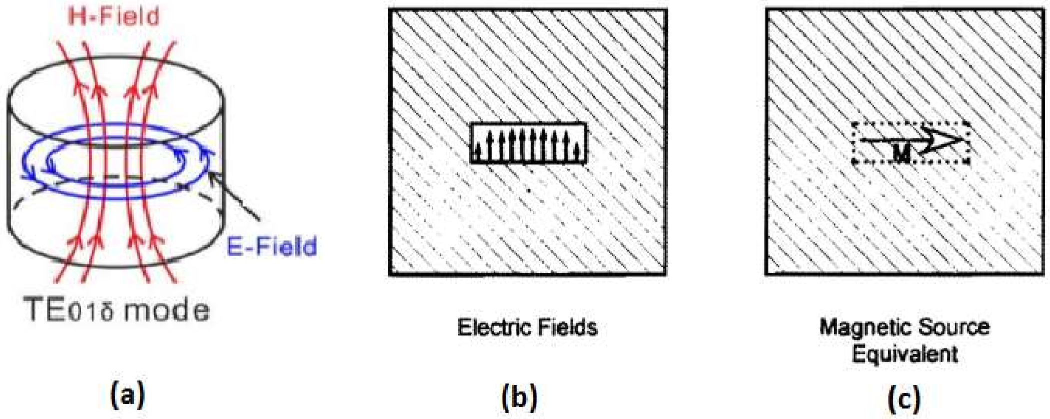

Figure 2.6: $TE_{01\delta}$ mode and excitation by slot feed [5] (a) electric and magnetic fields inside the cDRA for $TE_{01\delta}$ mode 3D view [10] (b) electric fields inside the slot. (c) Magnetic source equivalent for a slot feed

For $HE_{11\delta}$ mode, both probe and slots can be used. It was reported that probes were located at the wall of the cDRA to excite the cDRA as depicted in Figure 2.7 where the slot is located beneath the cDRA at the center or off-the-center [5].

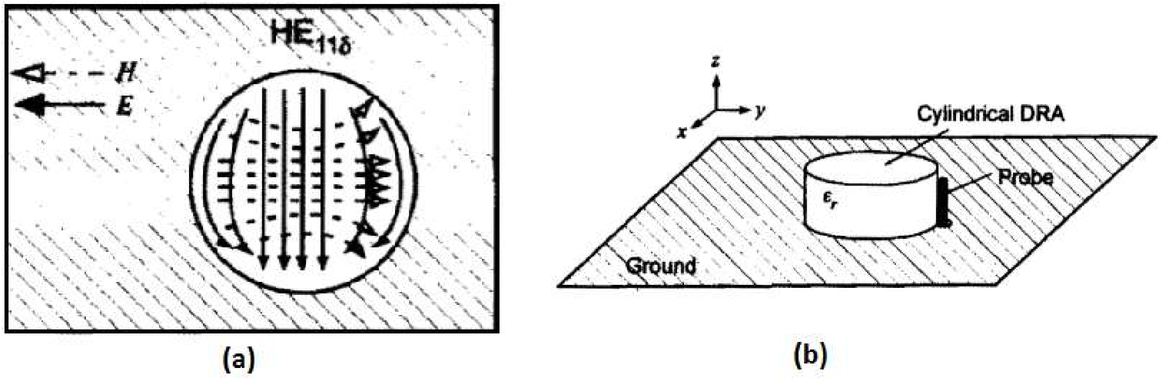

Figure 2.7 $HEM_{11\delta}$ mode and excitation by wall adjecet probe feed [5]: (a) electric and magnetic fields inside the cDRA (b) cDRA excited in its $HEM_{11\delta}$ mode by a side probe

2.3 MIMO Antenna Metrics

The MIMO antenna metrics of interest are the relations between the ports of the MIMO antenna system, namely, the Total Active Reflection Coefficient (TARC), Isolation and Correlation Coefficient.

2.3.1 Total Active Reflection Coefficient (TARC)

Individual reflection coefficients of the MIMO ports will not fully describe its behavior [3] and does not consider the effect of adjacent elements. Hence, the TARC is the ratio of the square root of the summation of the reflected power to the square root of the summation of incident power [4] as shown in (36) where a_i and b_i are the power of incident and reflected signals, respectively.

$$\Gamma_a^t = \sqrt{\sum_{i=1}^{N} |b_i|} \Big/ \sqrt{\sum_{i=1}^{N} |a_i|} \tag{2.37}$$

2.3.2 Isolation and Correlation Coefficient

As explained in chapter 1, the better the isolation between MIMO antenna ports, the better the performance of the MIMO antenna design. The isolation measures the coupling between the ports within the ground plane and in the substrate while the correlation coefficient measures the coupling of the channel in the air. An isolation of –10 dB between the scattering parameters S_{xy} is considered acceptable in densely packed antenna systems [4]. On the other hand, an envelope correlation coefficient (ρ_e) of 0.5 is considered acceptable. The envelop correlation coefficient (ρ_e) is approximately the square of the correlation coefficient (ρ) and is calculated from the radiated fields $F_i(\theta, \emptyset)$ by equation (37). For efficient antennas (95% efficiency and more), ρ_e can be calculated directly from the scattering parameters as shown in (38).

$$EC \quad = \rho_e = \frac{\left|\iint_0^{4\pi}\left[\overrightarrow{F_1}(\theta,\emptyset)*\overrightarrow{F_2}(\theta,\emptyset)\right]d\Omega\right|^2}{\iint_0^{4\pi}\left|\overrightarrow{F_1}(\theta,\emptyset)\right|^2 d\Omega \iint_0^{4\pi}\left|\overrightarrow{F_2}(\theta,\emptyset)\right|^2 d\Omega} \tag{2.38}$$

$$\rho_e = \left|\frac{\left|S_{ii}^* S_{ij} + S_{ji}^* S_{jj}\right|}{\left|(1-|S_{ii}|^2-\left|S_{ji}\right|^2)(1-\left|S_{jj}\right|^2-\left|S_{ij}\right|^2)\right|^{0.5}}\right|^2 \tag{2.39}$$

2.4 Summary

To summarize, basic antenna parameters were discussed. Definition and theory of operation of DRAs were introduced. A procedure for designing cDRA elements was presented. Fields and exciting the DRA were illustrated. Finally, important MIMO antenna metrics were discussed.

CHAPTER 3

LITERATURE REVIEW

DRAs have been well studied in the literature in the past four decades. One can classify them by shape: hemispherical, cylindrical, rectangular and others, or by band of operation: single band, multiband, wideband, and ultra-wideband, or by polarization: linear polarization or circular polarization. They can be categorized whether they are formed in an array, MIMO or single element configurations.

In this section, they will be divided into three categories: single DRA, DRA arrays and MIMO DRA configurations, and we will check what has been already reported in the literature compared to what we propose.

3.1 Single DRA

Most publications in the literature focused on the design and analysis of single element DRAs. The most shapes investigated are the cylindrical and rectangular shapes. Most focus was on modifying the DRA structure to obtain certain features such as exciting another mode to have dual band operation or to obtain circularly polarized radiation.

In [11], a novel technique was introduced to excite the higher order mode $HEM_{12\delta}$ in a cylindrical DRA. A non-centric air cavity under the cDRA altered the boundary condition which led to the excitation of the $HEM_{12\delta}$ mode. The cDRA had a gain of 9.5 dBi and resonated at around 7 GHz. The cDRA was probe fed and made of material with a dielectric constant of 10. A cDRA with a coating layer acting as a mirror was presented in [12]. The non-conductive coating layer had negligible effect on the operation of the DRA in both $TM_{01\delta}$ and $HEM_{11\delta}$ modes. For $TM_{01\delta}$ mode which was excited by a probe, the resonance frequency was shifted by 150 MHz from the designed resonance which is at 2.4 GHz when the radius of the DRA is larger than the radius of the ground plane.

Four rotated stacked rDRAs were proposed in [13] to obtain circularly polarized radiation. The design had an efficiency of 93% at the operating band of 1.7 GHz centered at 9.85 GHz. The four rDRAs were excited by a slot feed and mounted on top of one another with an angle of 30° between consecutive layers of the DRAs resulting in 90° difference between the bottom and top layers. The design could excite two degenerate modes TE^{x}_{111} and TE^{y}_{111}. The two modes are orthogonal to each other and their resonance is close which resulted in the circular polarization radiation pattern. Circular polarization was also obtained in [14] by introducing slits inside the rDRA as shown in Figure 3.1. This resulted in exciting an additional degenerate mode which made the CP realizable. The design was tuned for 5.2 GHz applications with bandwidth of only 210 MHz.

Dielectric Resonators (DRs) can be exploited for high efficiency small size on chip applications. In [15], an on-chip rDRA fed by a half mode cavity that exited higher order modes was presented. The rDRA was mounted on top of the chip and used to radiate in the millimeter frequency at 135 GHz. The antenna occupied small area of only (0.3 x 0.4) of the radiation wavelength as shown in Figure 3.2. Not only that, the efficiency of antenna was measured to be 62% with a maximum gain and fractional bandwidth of 3.7 dBi and 13% respectively. Another example was presented in [16] but in 60 GHz range. The design was slot coupled and achieved simulated efficiency of 98% and gain of 6 dBi with a fractional bandwidth of 6.1%. It was demonstrated that the measured results are affected by the RF front-end circuitry. The design uses Monolithic Microwave Integrated Circuit (MMIC) technology and is potential to be used in future 5G applications.

Another example of millimeter-wave at 60 GHz DRA was presented in [17]. The cDRA was surrounded by an Electromagnetic Band-Gap (EBG) structure. The advantage of the EGB is that it contributes to the radiation since high currents can be injected into it while suppressing surface waves. Along with the high efficiency cDRA, the design demonstrated a gain of 8.5 dBi (±0.7 dBi) from 57.2 GHz to 72.3 GHz.

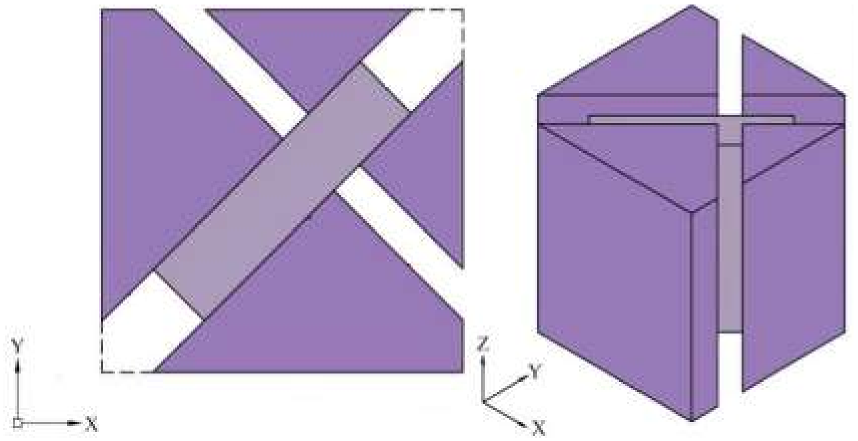

Figure 3.1: Slits in rDRA for CP operation [14]

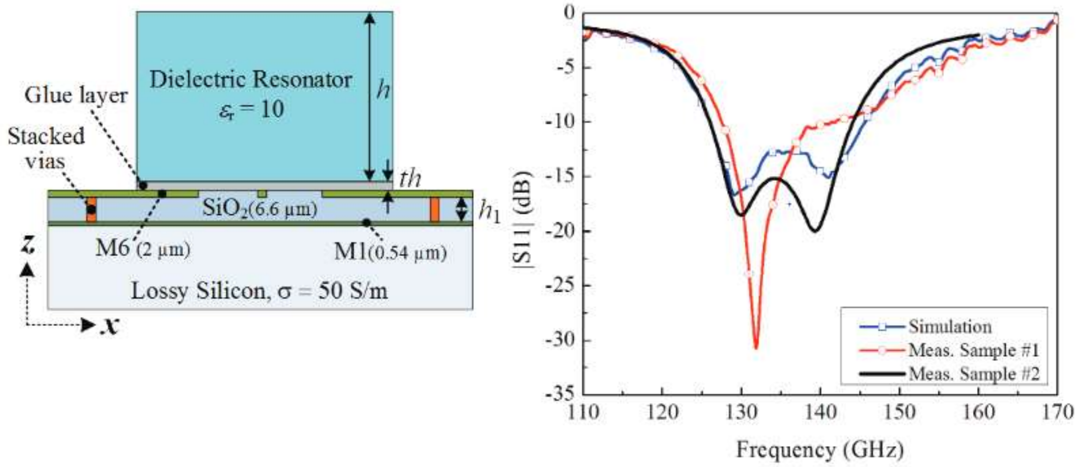

Figure 3.2: On-chip D-band rDRA and its reflection coefficient [15].

A dual band rectangular DRA was proposed in [18]. The rDRA operated at GPS (1.58 GHz) and WLAN (2.4 GHz) bands with fractional bandwidths of 6.3% and 3.68% respectively by introducing a groove and slits in the rDRA which resulted in generation of the two degenerate modes TE^{x}_{111} and TE^{y}_{111} for the GPS band as well as the degenerate modes TE^{x}_{113} and TE^{y}_{113} for WLAN band. The degenerate modes provided the design with circular polarization in both bands. A design technique was introduced in [19] for dual band probe fed cDRA. The fabricated cDRA is designed to resonate at WiMAX (3.5 GHz) and WLAN (5.8 GHz) with a gain of 1.3 dBi and 3.3 dBi, respectively, with Omni-directional radiation at both bands. A circularly polarized cDRA was presented in [20]. The cDRA was fed by a coaxial probe at its center from the bottom. It is also loaded on top with a circular patch that provided two functions: converting the linearly polarized fields from the cDRA into circularly polarized fields and resonating at a second independent frequency which made a flexible hybrid dual band design. [21] Proposed a dual band CP rDRA to be used in satellite applications at 3.08 GHz and 4.05 GHz. The antenna was fed by asymmetrical cross slot which was the key for the CP as well as the dual band operation. The design achieved a 2.3 dBi and 4.7 dBi gain in the lower and upper bands, respectively.

DRA Multi-band operation is achievable by exciting higher order modes. For example in [22], a cDRA excited by an aperture slot placed asymmetrically under the cDRA was presented. The cDRA was demonstrated to radiate in 11 different modes between 2.015 GHz and 4.29 GHz with a maximum gain of 3.6 dBi. It is worth noting that the high permittivity of this DRA (82.7) made the excitation of the higher modes possible. A band reject rDRA with ultra-wideband operation from 2.6 GHz to 12 GHz and the reject band is adjustable between 5 and 6 GHz was proposed in [23]. The band rejection was achieved by introducing two strips at the sides of the rDRA to alter the electric field distribution inside the cDRA in the notched band. Dual-cDRA design was proposed in [24] that provided an 8 dBi gain over wide band operation from 9.6 to 12.9 GHz with. The two cDRAs were fed by the same slot as shown in Figure 3.3 and were resonating in their $HEM_{11\delta}$ mode while occupying a total area of 30x25 mm^2.

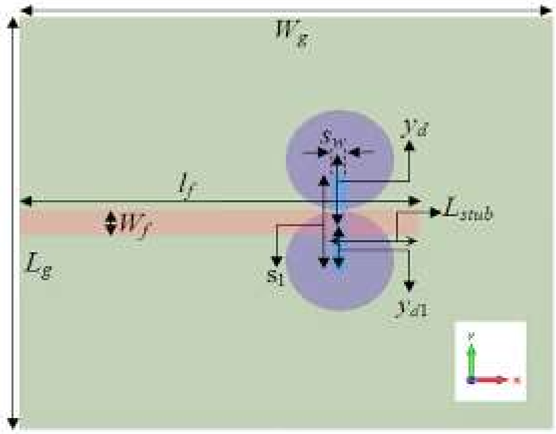

Figure 3.3: Two cDRAs fed by one slot for wide band operation [24]

DRAs were also investigated for usage in cognitive radio applications. In [25], an ultra-wideband (UWB) co-designed with a narrow band (NB) rDRA design was presented. The UWB-DRA covered the spectrum from 2.4 GHz to 12 GHz and was excited by a bevel-shaped patch mounted on the side while the NB radiated between 2.3 GHz to 4.5 GHz and was fed by a microstrip line. However, the design experienced -7dB isolation in the common operating band which is considered poor. Another example was presented in [26] where the UWB antenna was a U-shaped DRA fed by a microstrip line integrated with a NB slot antenna as depicted in Figure 3.4. The DRA can be used for spectrum sensing in the range of 2.94 GHz to 11.34 GHz while the NB antenna can be used for communication for the 5.8 GHz band (WLAN). Good isolation of -20 dB between the two ports was achieved. A wide band hybrid antenna was presented in [27]. The structure was made of an rDRA excited by an annular (ring) slot with common center point. Four branches are extended from the slot as shown in Figure 3.5 to excite circularly polarized modes in the rDRA. The slot also acts as an antenna which adds another resonance frequency to the structure that led to a wideband operation from 2.2 GHz to 2.9 GHz with average gain and efficiency of 5 dBi and 95% respectively.

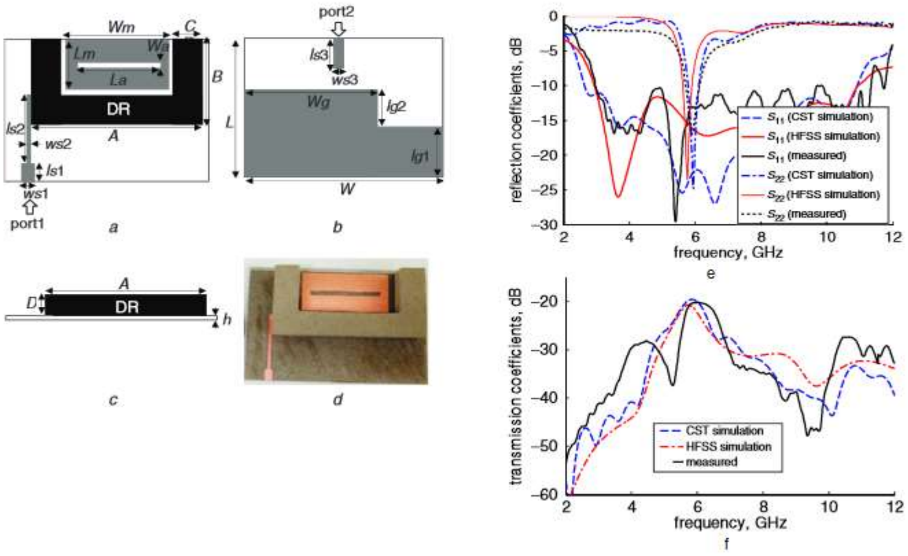

Figure 3.4: UWB hybrid (U-shape DRA and slot antennas) and their performance [26]

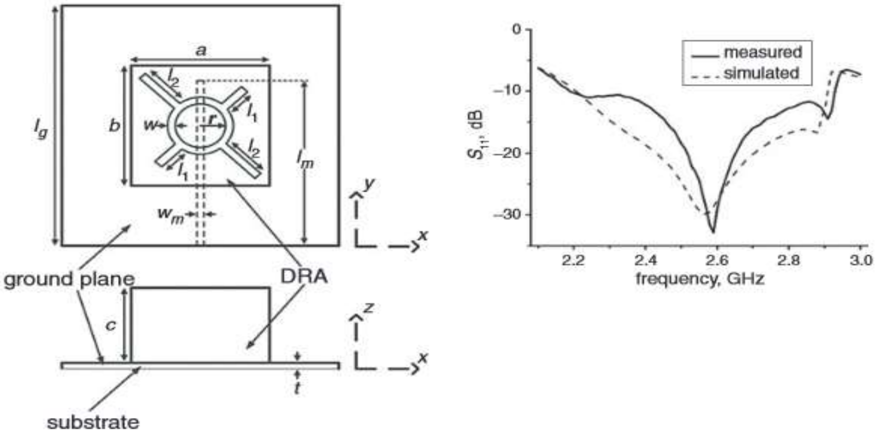

Figure 3.5: wideband rDRA excited by an annular slot and its reflection coefficient [27]

An enhanced bandwidth DRA for WiMAX applications is realized by a two layer hemispherical DRA (hDRA) made of two transparent materials (glass and acrylic) as shown in [28]. Design formulas were modeled and validated. The measured results showed good agreement with the formulas. The design covered a fractional bandwidth of 31.9% with center frequency at 3.3 GHz. An inverted hDRA –or cup shape- fed by a probe from its center was demonstrated in [29]. The design covered a wide band from 1.9 GHz to 3.6 GHz with an average gain of 3.5 dBi. An UWB dual conical shape DRA was presented in [30] to cover a wide range of the spectrum from 2.8GHz to 15.2 GHz (138% fractional bandwidth). The two DRAs had different dielectric constant, fed by common probe from the center which contributes to the radiation (hybrid antenna) and were stacked on top of one another with two configurations as shown in Figure 3.6. The maximum gain achieved was 8 dBi. A similar technique to [14] was proposed in [31] for wideband operation. In addition to the slits, tampered ground and feed as well as a matching resistor were utilized to achieve the target bandwidth. The design demonstrated 36% fractional bandwidth around 3.7 GHz with a gain of 6 dBi.

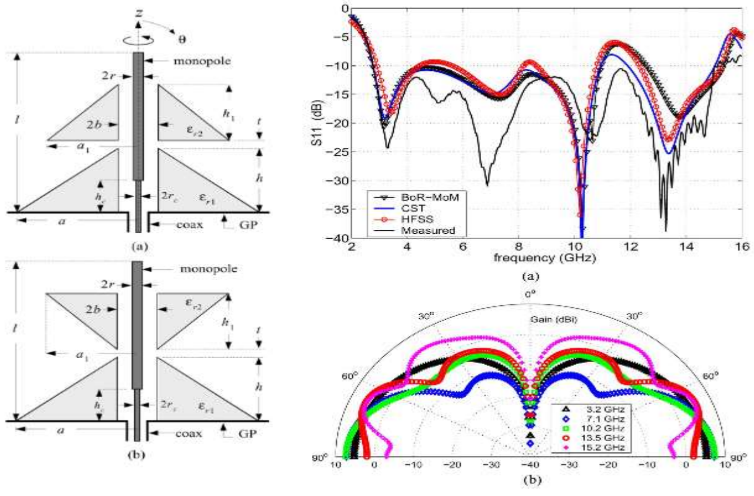

Figure 3.6: UWB conical-shape DRAs and their performance [30]

Non-conventional shapes for the DRA and their feed were reported –as an example- in [32] where a ring-shape DRA was fed by in monopole antenna form. UWB operation was recognized between 3.49 GHz and 7.2 GHz as depicted in Figure 3.7 with an average gain of 4.31 dBi.

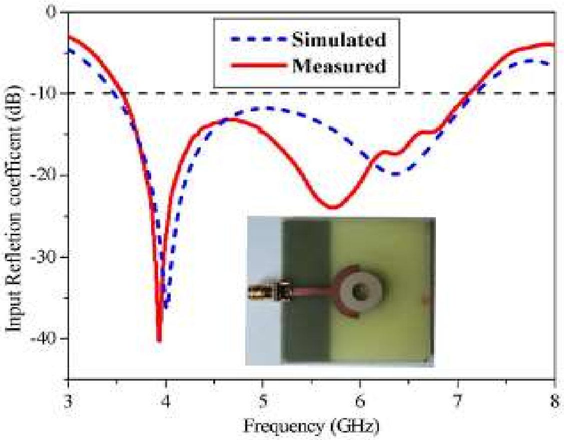

Figure 3.7:UWB ring DRA excited by a semi-annular microstrip [32]

DRAs also offered diversity in frequency and polarization. For example, [33] proposed a three port polarization diversity cDRA. The cDRA resonating at 2.4 GHz and fed by a probe at the center and two pairs of balanced slots is shown in Figure 3.8. Using this innovative technique, it was possible to excite TM$_{01\delta}$ resulting in an Omni-directional radiation, HEM$^{x}_{12\delta+1}$ and HEM$^{y}_{12\delta+1}$ resulting in broadside radiation. The microstrip lines were extended beyond the slots for impedance matching while it was done by varying the probe length. A maximum envelop correlation coefficient was calculated from the S-parameters and was around 0.0015 in the operating bandwidth. A two port cDRA was presented in [34], the top surface of the cDRA was loaded with a circular patch with extended branches and fed from the bottom with an axial probe as port 1 and slot as port 2 as shown in Figure 3.9. The design was successful in exciting TM$_{01\delta}$ mode that is converted to a CP radiation by the patch and the two degenerate modes which resulted in another CP radiation that was of a low correlation with the first one. At 2.45 GHz, the efficiency of the design was above 70% with an envelope correlation coefficient of 0.001.

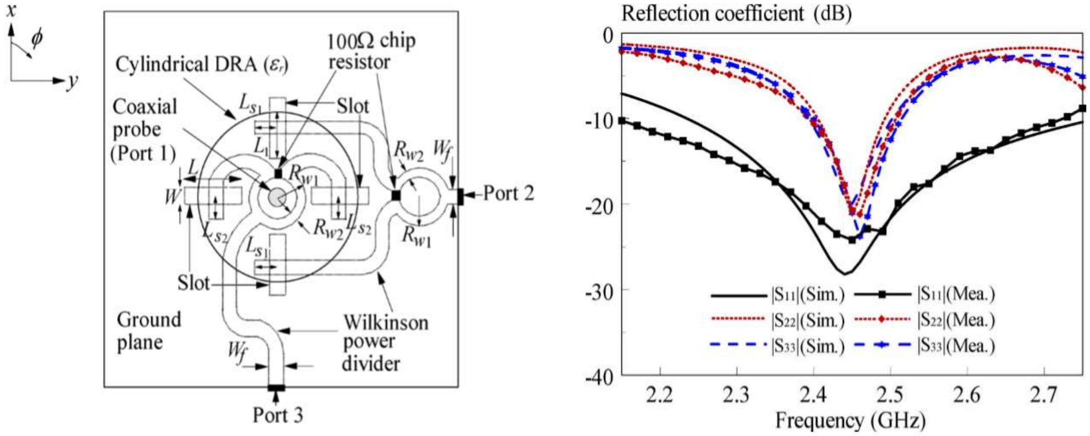

Figure 3.8; Three-port polarization diversity antenna [33]

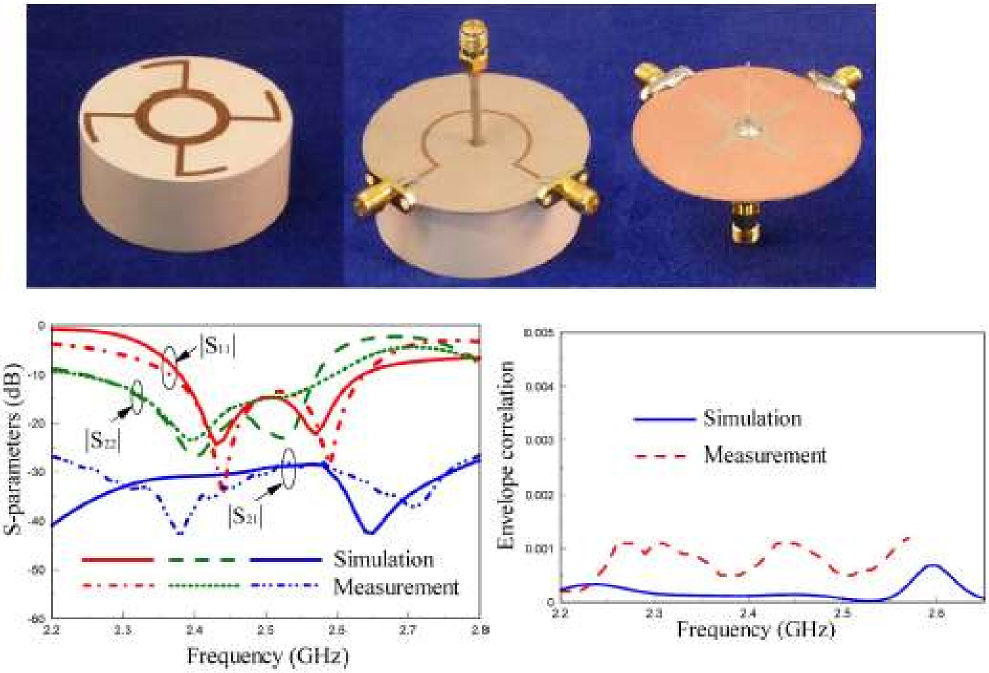

Figure 3.9: Pattern Diversity cDRA loaded with circular patch and its performance [34]

In [35], frequency configurability was achieved by introducing air channels between the slot coupled rDRA and the ground plane. The switching in frequency was realized by adding metallic slugs beneath the DRA filling parts of the air channels as illustrated in Figure 3.10. The lower and upper frequencies were 16.7 GHz and 21.4 GHz with bandwidths of 6.1% and 9.7% and gains of 4.9 dBi and 5.8 dBi respectively. However, the switching was done mechanically which is impractical. On the other hand, a frequency agile rDRA was presented in [36] where switching was made electronically using pin and varactor diodes for discrete and continuous switching respectively. The design utilized metallic walls on the sides of the rDRA that were activated and deactivated by the diodes. This mechanism intends to change the fields inside the rDRA which will result eventually in shifting the resonance frequency. The design reported a tuning range of 91% and 55% for discrete and continuous switching respectively in the frequency band of 2 to 7 GHz.

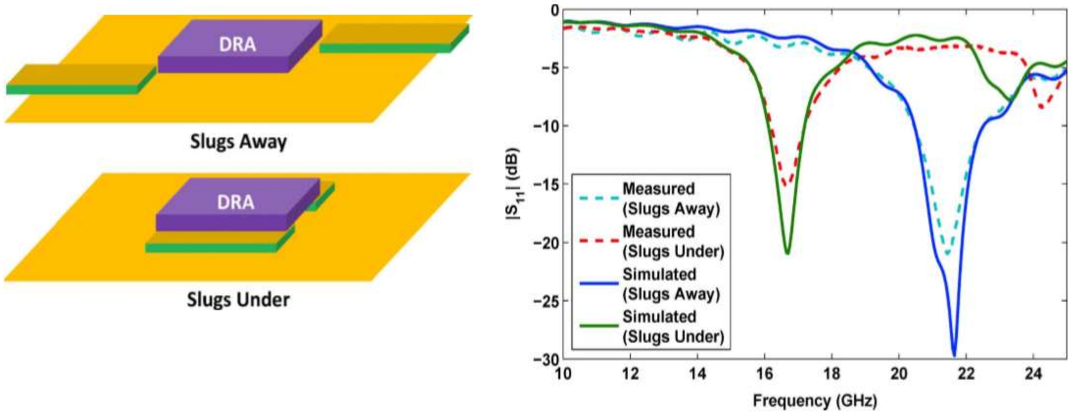

Figure 3.10: Frequency configurability by air channels and metallic slugs [35]

3.2 DRA Arrays

Compared to single DRAs, DRA arrays were investigated in the literature with lesser magnitude. The research in DRA arrays focused on designing high efficiency structures for mm-wave as well as radiation steering and beam scanning applications.

Since the bottleneck of efficiency is the feed network when it comes to mm-wave DRA array design, [37] presented and modeled a unique way for linear mm-wave DRA array designs. The antenna elements of the array were excited by the two configurations of slots. Slots are openings on the top surface of Substrate Integrated Waveguide (SIW) as shown in Figure 3.11. The substrate is used as waveguide by introducing metallic vias on the two sides acting like side walls of a metallic waveguide along the direction of propagation while the top and bottom layers are coated with metal (copper). The spacing between the vias are optimized to reduce the losses. The 4x1 SIW-rDRA achieved a gain of 11.4 dBi across impedance bandwidth of 4.7% around 33.8 GHz with high efficiency of 90%. A steerable rDRA array for Radar scanning was proposed in [38]. The geometry was composed of three rDRAs where the first and third were loaded with reactive loads (capacitors) and the second is fed by a conventional microstrip line as shown in Figure 3.12. By changing the value of the capacitors, the design could achieve ±30 degrees steerable radiation with a stable gain of 7 dBi at 2.8 GHz and 130 MHz bandwidth. Another example of radiation steering by DRA arrays was presented in [39] where a seven element hDRA array was analyzed. The elements were arranged in a hexagonal distribution with elements at the corners and the center of the hexagon.

A third example was presented in [40] for a four element phased rDRA array coupled to slot feeds. Changes in the phase were realized electronically by liquid crystal phase shifters. The design achieved a beam steering of at least ±30° at 10 GHz as shown in Figure 3.13.

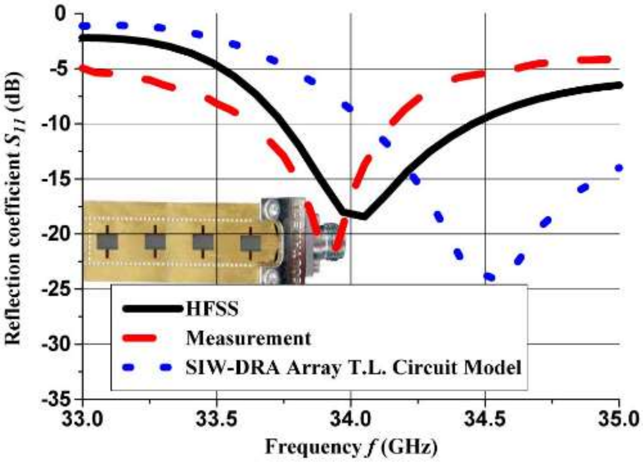

Figure 3.11: SIW-rDRA array for mm-wave applications [37]

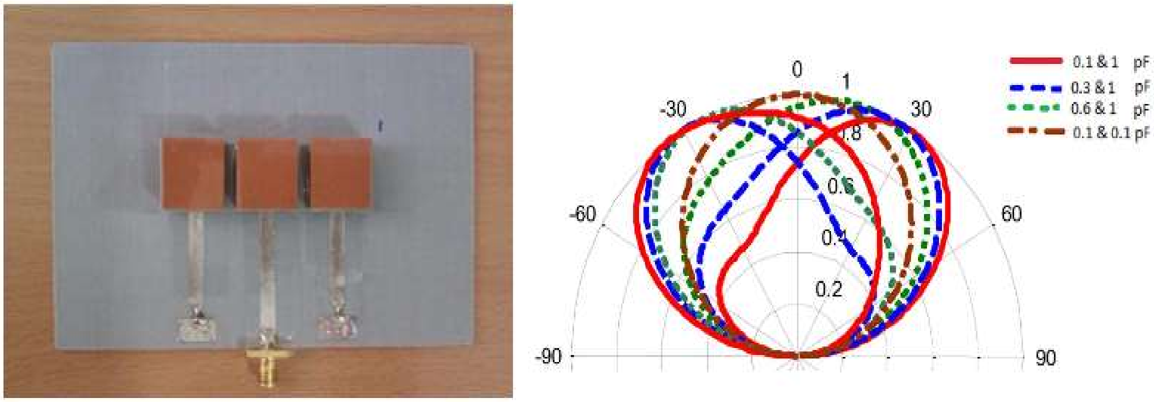

Figure 3.12: Pattern steering using phased rDRA array [38]

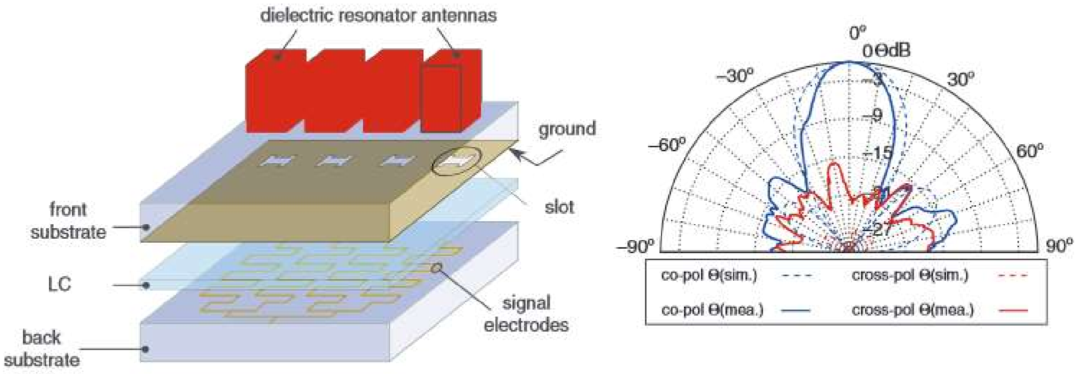

Figure 3.13: rDRA phased array with LC phase shifter and steering performance [40]

A dual band triangular DRA made of two elements was proposed in [41]. The array was designed for WiMAX and WLAN applications. The simulated design achieved maximum gains of 7.0 dBi at 3.5 GHz and 8.9 dBi at 5.2 GHz. A nine-element cross-shaped DRA array was proposed in [42] . The arrays were designed to radiate at 60 GHz where each element is fed by rectangular slot. A superstrate was added at a distance of 1.23mm from the top of the DRA elements to enhance the gain which was obtained from the simulation to be 19-21 dBi for a wideband of 9.8%.

3.3 MIMO DRAs

One can find few MIMO DRA based in the literature. Combining the advances of MIMO antennas with DRAs efficiency has been exploited in [43] where a two three-port DRAs for WLAN was presented. The design showed not only spatial diversity as in conventional microstrip MIMOs but also in polarization and radiation patterns. This was feasible due to the fact that a single DRA can be excited by numerous techniques as was shown previously in [33]. The advantage of the design was its compactness (only 2 elements) compared to conventional printed MIMO structures where 6 elements is usually needed for such configuration. The design achieved a minimum measured channel capacity of 9.0 bps/Hz at 10 dB signal-to-noise ratio.

In [44], a two-port one element semi-cDRA was presented as a MIMO structure. The design was tuned to resonate in $TE_{011+\delta}$ and $HEM_{11\delta}$ modes at the same frequency (720 MHz). The measured isolation was -30dB with channel capacity of 11.1 bps/Hz. However, the bandwidth of the two modes is considered low (less than 35 MHz). No information about the correlation coefficient was presented.

A dual polarization cDRA was presented in [10] as a MIMO structure. The design excited the orthogonal modes $TM_{01\delta}$ (using a probe) and $TE_{01\delta}$ (using curved microstrip lines) as shown in Figure 3.14 which resulted in horizontal and vertical polarizations. Some techniques were used to enhance the impedance matching –and hence the bandwidth- such as elevating the cDRA to introduce an air-gap and adding a cap to the feeding probe. The design achieved an overlapping bandwidth of 7.4% centered around 3.9 GHz. The envelop correlation coefficient (ECC) was less than 0.005 in the band of operation.

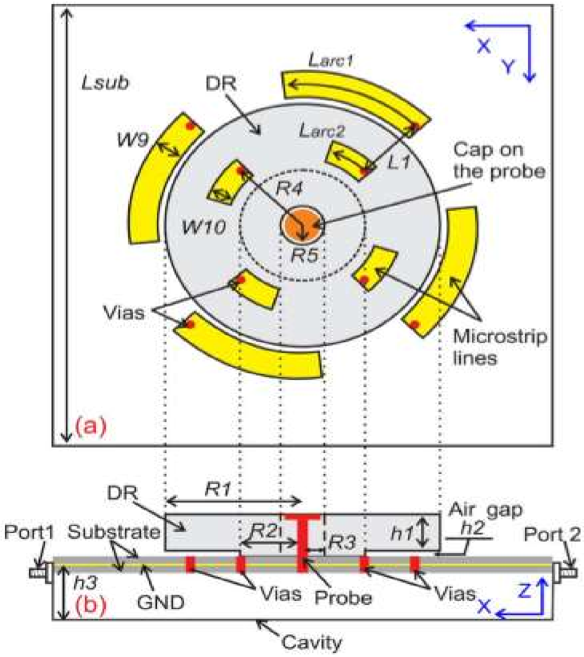

Figure 3.14: MIMO cDRA fed by a probe and curved microstrip lines [10]

Another two-port one element cDRA MIMO was presented in [45]. The key to the MIMO implementation in this design was the excitation of two opposite $\mathrm{HEM}_{11\delta}$ modes from two orthogonal feeds as depicted in Figure 3.15. The structure was resonating at 4.07 GHz with 2.7% bandwidth and -13.4dB isolation between the two ports. The design achieved a channel capacity of 5.03 bps/Hz for the Line-of-Sight scenario compared to a theoretical capacity of 5.17 bps/Hz.

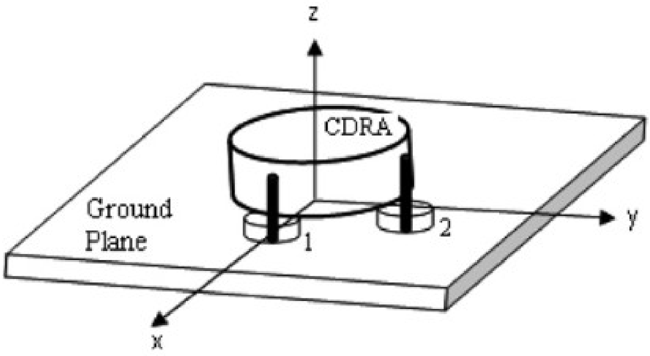

Figure 3.15: MIMO cDRA excited by two orthogonal feed [45]

A frequency agile DRA MIMO was presented in [46]. The design can be used in modes: MIMO for enhancing channel capacity where the ports operate at the same frequency and frequency switching between the two independently. The targeted modes of the cDRA were $TE_{011+\delta}$ and $HEM_{11\delta}$. The antenna geometry is shown in Figure 3.16. The design is operating in MIMO mode while being tuned for a range of frequencies from 622 MHz to 780 MHz (30% tuning ratio). The lowest isolation measured was -14.4 dB.

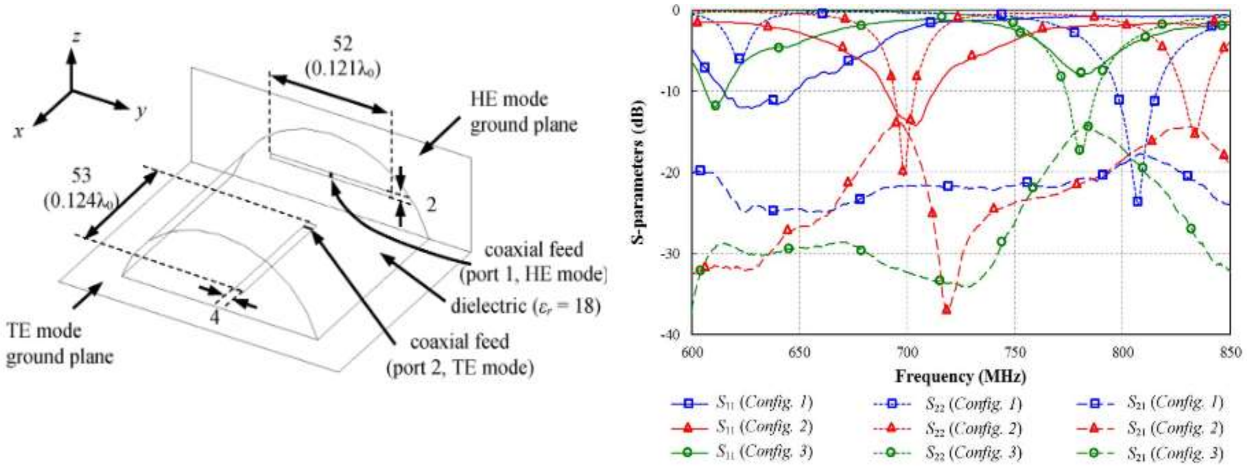

Figure 3.16 Frequency Agile cDRA MIMO and its reflection coefficient [46]

Based on the above classification of DRA (Single, array or MIMO configurations),

Figure 3.17 shows a tree summary of the literature review. A further breaking down is based on the band of operation (single band, dual or multi band and wide or UWB). The latter was further divided according to their resonance frequencies (greater than or less than 12 GHz).

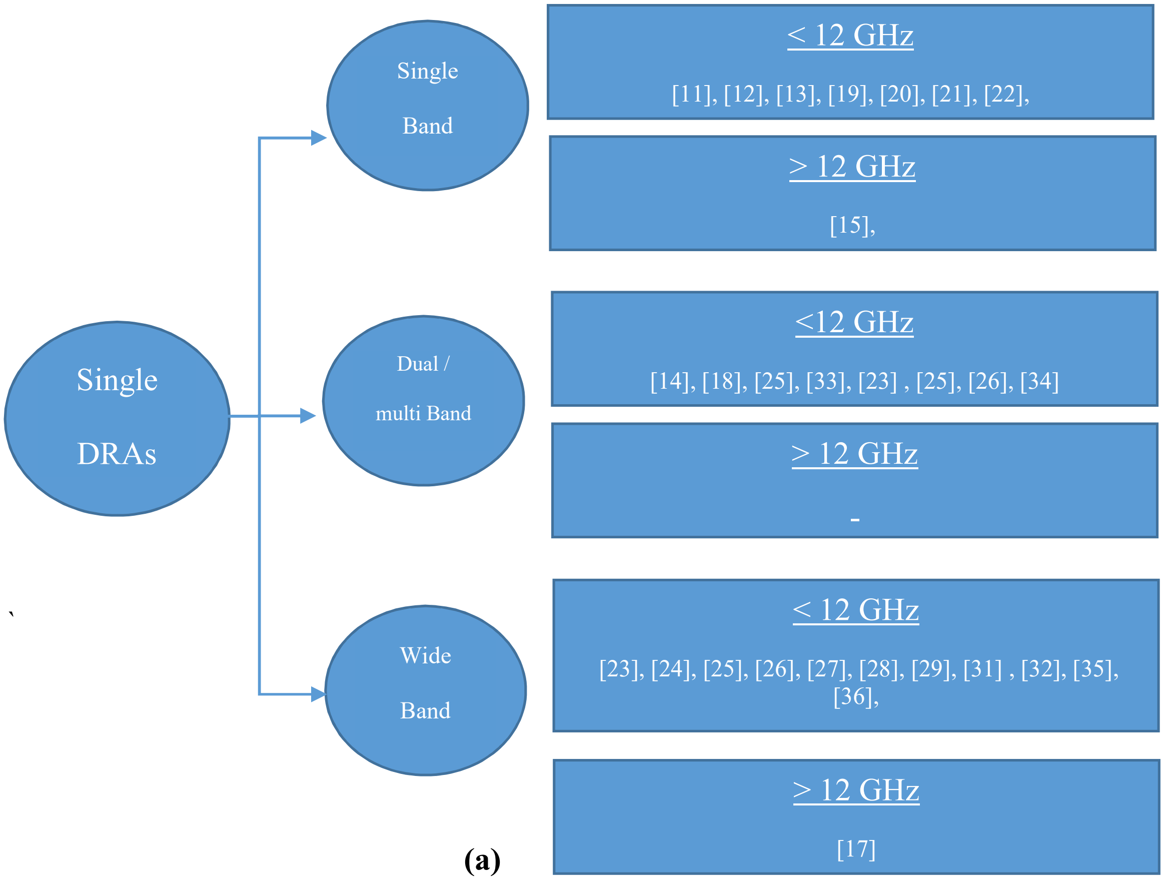
Single DRAs
Single Band
Dual / multi Band
Wide Band
< 12 GHz
[11], [12], [13], [19], [20], [21], [22],
> 12 GHz
[15],
<12 GHz
[14], [18], [25], [33], [23] , [25], [26], [34]
> 12 GHz
-
< 12 GHz
[23], [24], [25], [26], [27], [28], [29], [31] , [32], [35], [36],
> 12 GHz
[17]

(a)

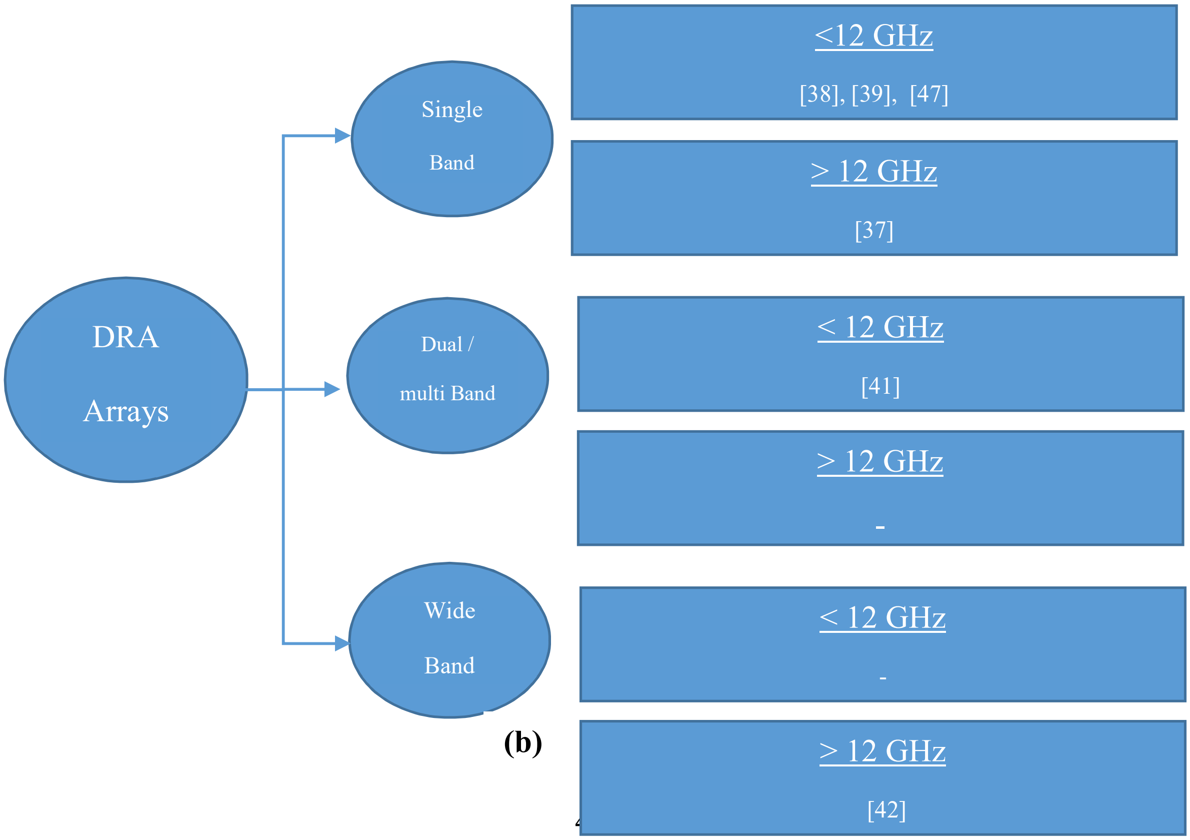
DRA Arrays
Single Band
Dual / multi Band
Wide Band
<12 GHz
[38], [39], [47]
> 12 GHz
[37]
< 12 GHz
[41]
> 12 GHz
-
< 12 GHz
-
> 12 GHz
[42]

(b)

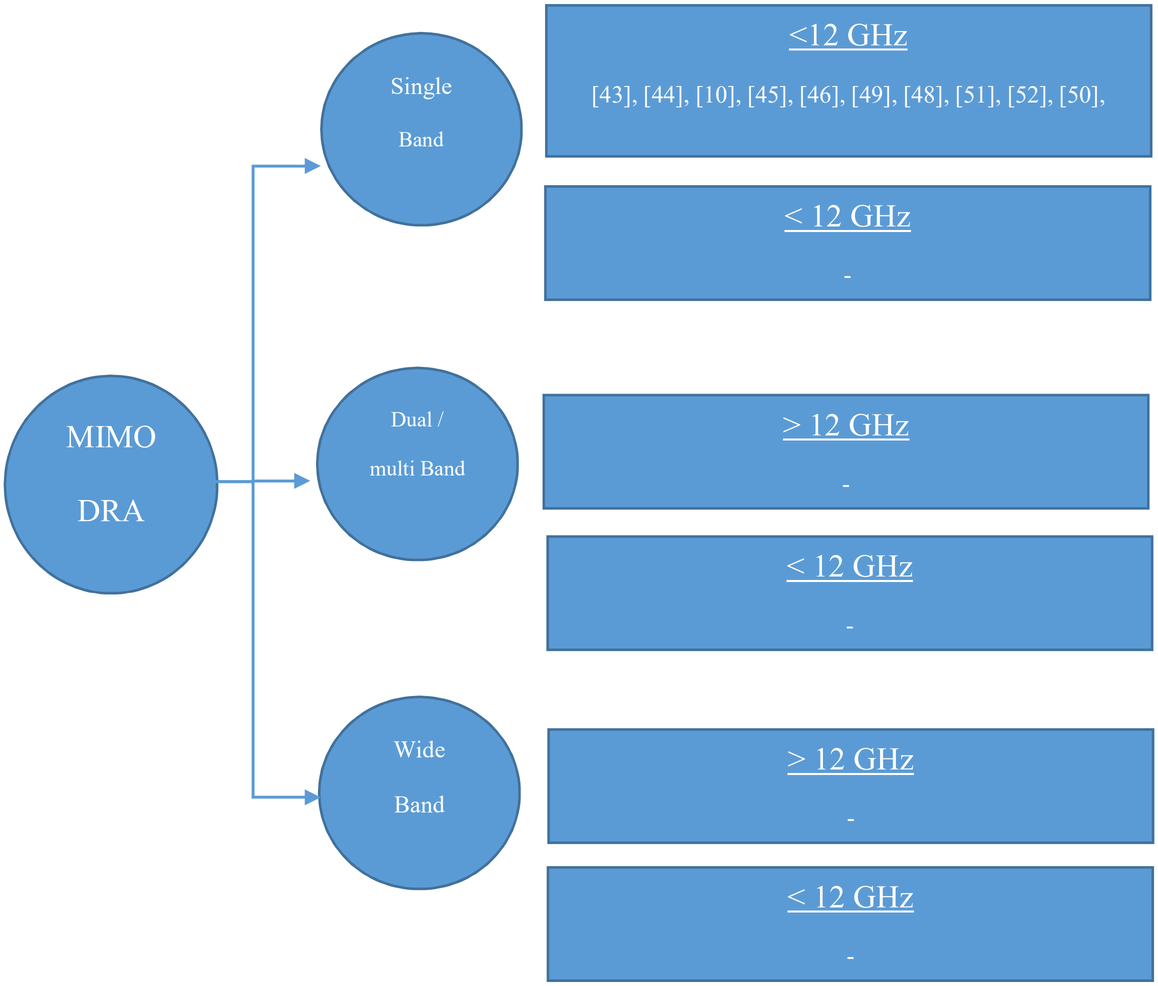

(c)

Figure 3.17: Literature review summary tree (a) Single DRA (b) DRA arrays (c) MIMO DRAs

As can be noted from the tree in

Figure 3.17, very few works targeted DRA based MIMO systems. All of the MIMO DRA based designs covered frequencies less than 12 GHz. Very few designs utilized DRAs for frequencies above 12 GHz. There is no design combined MIMO and array configuration to obtain both high gain and steerable radiation pattern in the mm-wave range was proposed before.

CHAPTER 4

TWO-ELMENET MIMO CDRA ARRAY DESIGN

In this chapter, the design of a MIMO cDRA-based system operating in the mm-wave band of 30 GHz is explained in details. The design steps and results using the commercial software ANSYS HFSS are shown. The design is divided into five steps:

1. Single cDRA design.
2. Four-element cDRA array with tuned input phases.
3. Two port MIMO cDRA-based Antenna System
4. Feed network design.
5. Integration of feed network and antennas to construct the full design.

4.1 Single cDRA Design

Following the design steps presented in chapter 2, the targeted cDRA was designed to satisfy the following requirements:

1. Center frequency: 30 GHz.
2. Bandwidth: 1 GHz

Since the objective is to fabricate the design, it was taken into consideration the available material from which the cDRA will fabricated. The available material was Hik500 with $\varepsilon_r = 10$ and $\tan\delta = 0.002$.

Following the procedure in 2.2.3, we start with dimensions a=2mm, h=3mm. With ε_r=10, we evaluate equations (8) and (14) for $TE_{01\delta}$ and $TE_{011+\delta}$ modes to calculate ($k_o a$) and then substitute in (3) and (7) to calculate f_o. We obtain:

$TE_{01\delta}$: f_o= 19.05 GHz Q=7.37

$TE_{011+\delta}$: f_o= 23.3 GHz Q=17.24

We notice that the $TE_{011+\delta}$ mode is closer to the target frequency. It is expected that by reducing the aspect ratio (a/h), the calculated frequency will increase. Table 2 shows the calculations made to find the suitable dimensions of the cDRA. It is noted that in all iterations, the criterion for the aspect ratio (0.5≤ a/h ≤5.0) is not violated according Table 1.

Table 2: f_o and Q for TE011+δ mode for different aspect ratios (a/h)

a (mm)	**h (mm)**	**a/h**	**f (GHz)**	**Q**
2	3	0.67	23.3	17.24
1.8	3	0.6	25.07	16.13
1.6	3	0.53	27.28	14.73
1.5	3	0.5	28.61	13.93

1.6	3.1	0.52	27.04	14.33
1.4	2.8	0.5	30.65	13.93

It should be noted that results obtained in Table 2 are starting approximations because of three reasons: the first is that the equations are derived from approximate solutions of the fields in the dielectric resonators. There is no closed form solution for the fields in the cylindrical DRA. Second reason is that the equations do not take into consideration the loading effect on the DRA from the feed network which is expected to shift the center frequency and add limitations on the bandwidth. Third, the equations are based on infinite ground plane assumption.

DRAs can be mounted on modern PCBs and interfaced with the RF front-end circuitry with a variety of feedlines. Examples are: microstrip lines, aperture coupling, probe feed…etc. As with patch antennas, aperture coupling is expected to provide larger bandwidth to the antenna. Not only that, the targeted modes to be excited are the transverse electric modes which are best excited by a magnetic current source which is realized by slot coupling. Hence, aperture coupling was selected as the excitation mechanism for the antenna system.

A single cDRA was modeled in Ansys HFSS to validate the design. Figure 4.1 shows the schematic of the single DRA and its model in HFSS. A parametric sweep is conducted in order to tune the dimensions of the cDRA to the desired frequency and bandwidth.

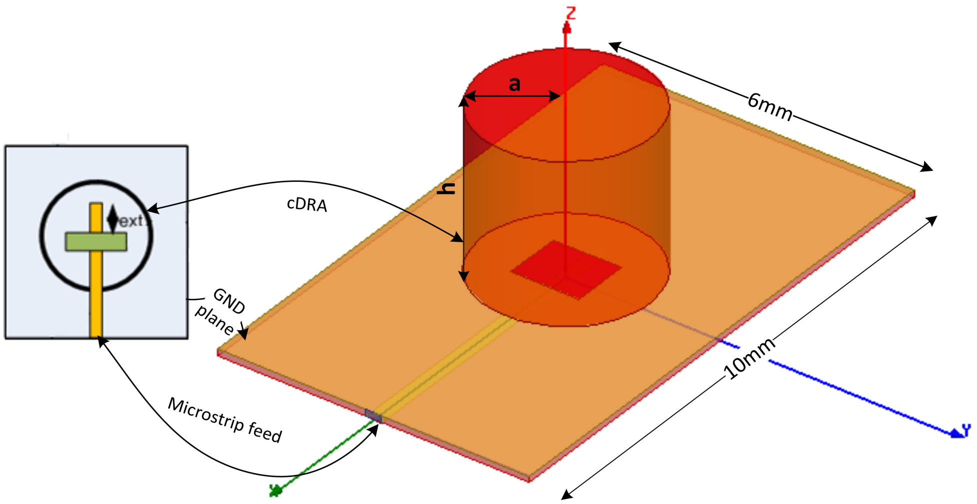

Figure 4.1: Single cDRA schematics

A parametric study in HFSS is conducted to tune the dimensions of the cDRA. The feed line was extended by 1mm beyond the center of the cDRA for impedance matching. The reflection coefficient curves for different values of a and h are shown in Figure 4.2. It is noted that the closest match to the target design was achieved when a=1.6mm and h=3.1mm.

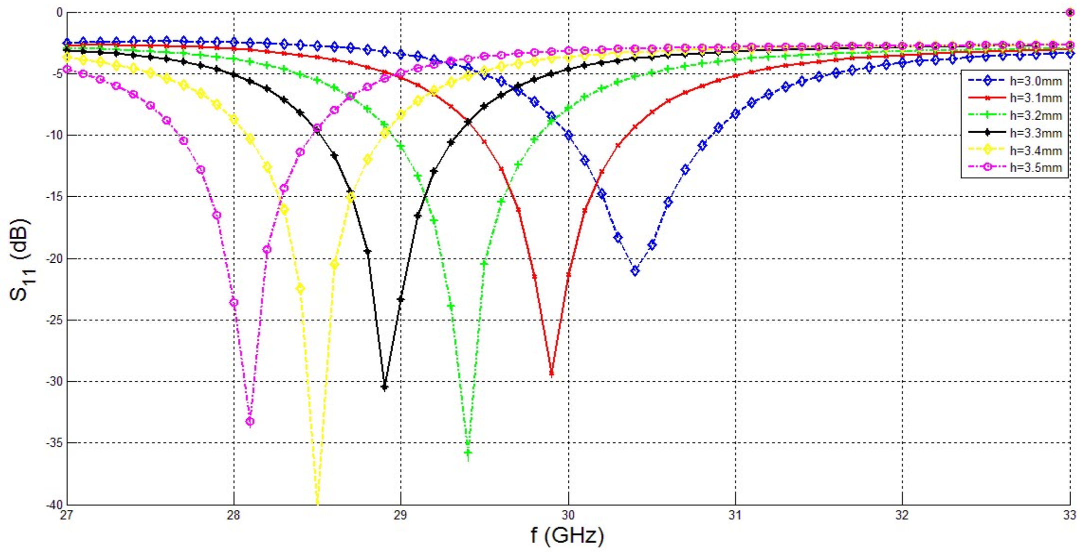

Figure 4.2: Reflection Coefficient Parametric study for different cDRA heights

Figure 4.3 shows the radiation pattern of the single cDRA. It is worth noting that at this high frequency, the radiation efficiency is 95% and the maximum gain obtained for a single DRA is 4.8 dBi.

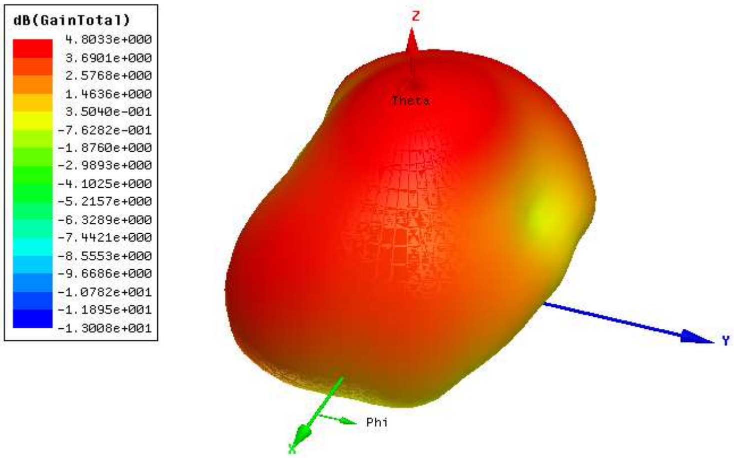

Figure 4.3: Radiation Pattern of a single cDRA at 30 GHz $TE_{011+\delta}$ mode

4.2 Four-element cDRA array

The single cDRA design is used to construct an array of four elements. This step is essential before constructing the complete MIMO system and the feed network. The main aim is to tune the phases of the input signal of each cDRA element in order to achieve a beam tilt of 45°. Tilting the beam to this angle is expected to result in enhanced channel isolation between the input ports of the MIMO system and low correlation between the MIMO ports which are the key factors in good MIMO behavior.

In order to preserve the compactness of the design, the inter-element spacing in one array is kept at 6 mm from center to center. The array was created in HFSS with four input signals to control their phases and tune the resulted beam towards 45 degrees with the azimuth. Figure 4.4 shows the 3D model of the array in HFSS. The optimum phase difference between the input signal of consecutive cDRAs -from left to right- was found to be 153^o to generate a 45 tilt in the beam with the azimuth.

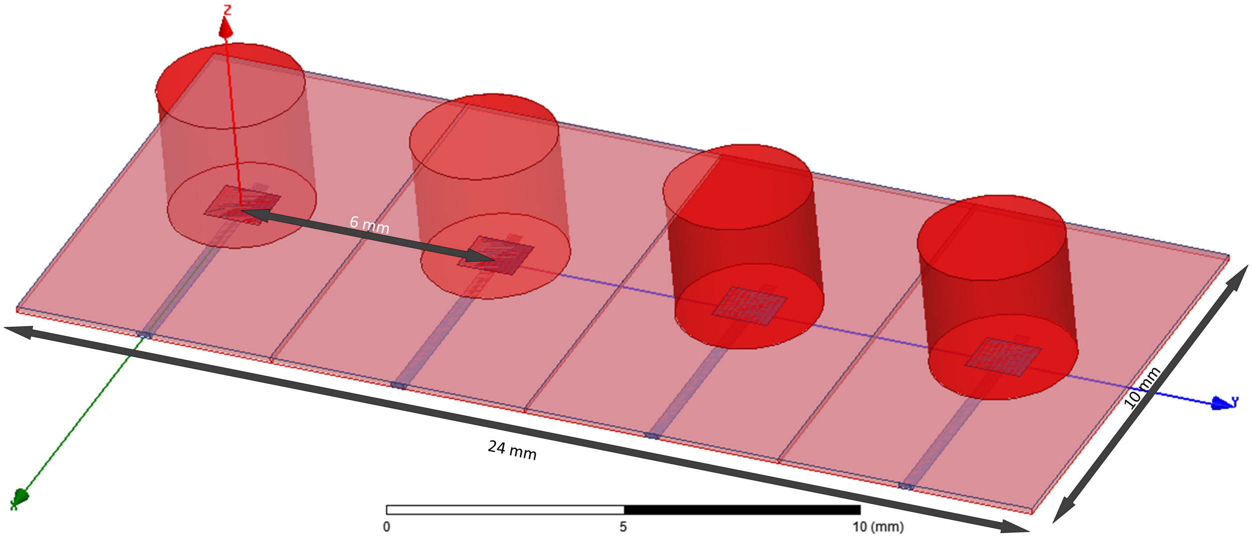

Figure 4.4: Four-element cDRA Array in HFSS

4.3 Two port MIMO cDRA-based Antenna System

The two port MIMO design is composed of two linear cDRA arrays. Each array consists of 4 DRA elements. The elements are placed at a distance of 6.0mm from their centers for better isolation while maintaining a compact design. The two arrays are placed linearly with a distance of 6 mm. An array for each port was chosen to be able to control the beam pattern to achieve a good correlation coefficient. To validate the design, the MIMO antenna system is modeled in HFSS without the feed network. Assuming proper excitation provided at each port, the radiation Patterns obtained showed the main lobes is tilted approximately 45° to the left and right (in theta plane) for the left and right arrays respectively. This will result in low correlation as will be shown in section 4.4. It is noted that each array achieves a maximum gain of 9 dBi while maintaining efficiency higher than 95%. Shows the gain patterns of the two MIMO ports and clearly the beam tilts are identified.

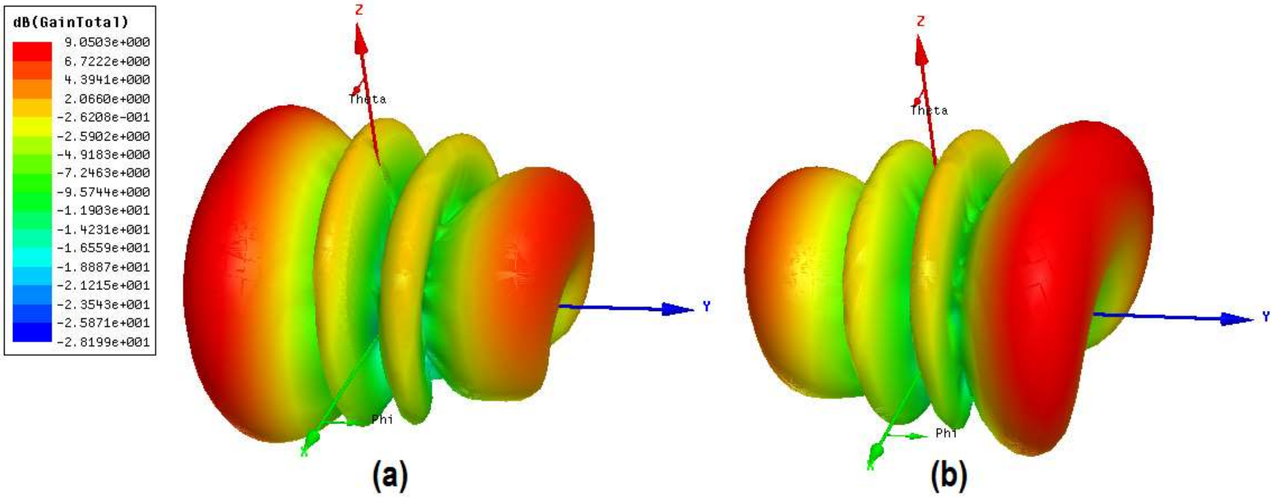

Figure 4.5: Radiation Pattern for cDRA MIMO (a) left array (b) right array

4.4 Feed network design

A passive feed network is designed to achieve the design objectives. As explained in the previous section, the feed network is required to provide the cDRA elements with phase difference in the input signal of 153°. The signal should be divided equally between all branches. T-shape microstrip power dividers was adopted to design the feed network. Hence, the following points were considered while designing the feed network:

- Maintaining fixed distances between final branches of 6mm.

- Maintaining impendence matching after branching. Quarter wavelength transformers of 70.7 ohm were used to match the branched 50 ohm lines.
- Introducing the required phase shifts by introducing meadner-lines like before feeding the signal to the cDRA elements.

The top layer of the system PCB is a large ground plane. The cDRA elements are fixed on top of the ground plane. Coupling to the cDRAs is realized by openings (slots) in the ground plane beneath the center of the cDRA where strong magnetic field can be excited. The size of the slot was optimized to be 1.1mm x 1.3mm. To minimize the losses from the network at this high frequency, a low loss thin substrate is used. Rogers RO3003 of ϵ_r=3, loss tangent of tanδ=0.002 and thickness of 0.13mm is used as the system substrate. The feed network is placed on the bottom side of the system PCB. The feed network will have two ports for two port MIMO antenna system operation. Each port will branch to four lines to feed each cDRA element. The required feed network will have two functions: an equal one-to-four power divider and a passive phase shifter. To achieve the 45° tilt in the radiation, the progressive phase between consecutive branches should be ±153°.

Figure 4.6 shows the schematic of the proposed complete MIMO antenna system including the feed network and the DRA elements. It also shows the placement of the cDRA elements. The thick lines are 50Ω while the thin lines are 70.7Ω to provide proper matching for the power dividers/combiners. Microstrip line widths are 0.3mm and 0.18 mm for 50 Ω the 70.7 Ω respectively. The 50Ω lines are used for signal transmission while the 70.7Ω lines are λ/4 transformers. Before the end of each branch, zig-zags (meandering) are made in the transmission lines to realize the required phase shifts. Taking into consideration the 6mm distance between each line from center to center, trade-offs were made to come up with the final design.

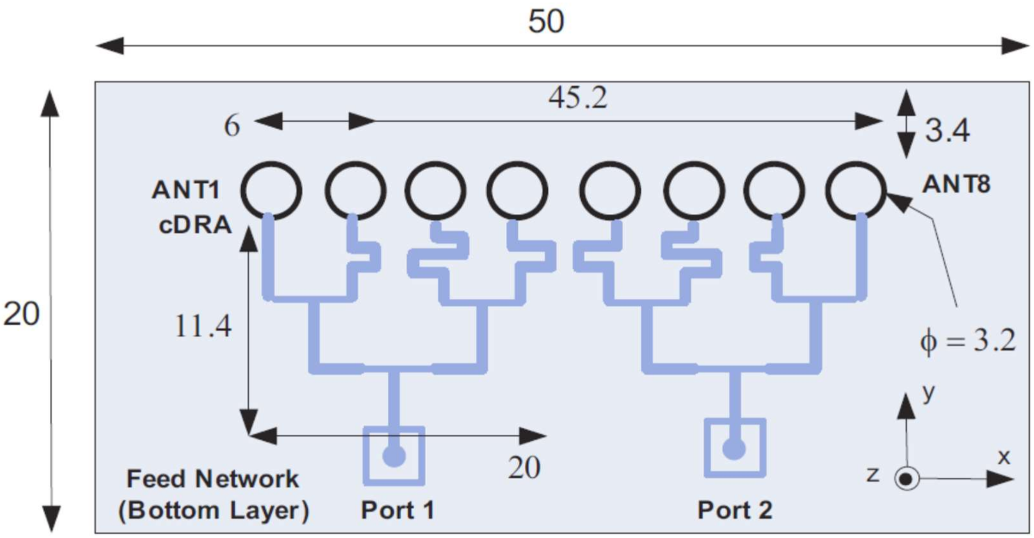

Figure 4.6: Schematics of the complete design (bottom view)

Table 3 shows the required theoretical and the obtained (modeled/simulation results) magnitude and phase from each branch of the feed network without antennas at 30 GHz. Ports 1 to 4 are the output ports where port 1 has no phase shift from the input. As expected for longer lines, losses are greater. A trade-off between magnitude and phase was considered. The maximum error obtained for the magnitude is 2.3 dB while the maximum error obtained for the phase is 28°.

Table 3: Theoretical and simulated output signals of the feed network (magnitude and phase)

Parameter	**Port 1**	**Port 2**	**Port 3**	**Port 4**
Magnitude for ideal case (Watt)	0.25	0.25	0.25	0.25
Simulated Magnitude (Watt)	0.268	0.199	0.136	0.178

Ideal Case relative phase shift (degrees)	0	153	-54	99
Simulated Phase shift (degrees)	0	155	-26	120

The feed network shows stable performance over the band of operation (from 28 GHz to 32 GHz). Figure 4.7 and Figure 4.8 show the magnitude and phase of the output signals from one complete feed network over the desired band where port 1 is the input port and ports 2 to 5 are the output ports. A maximum error of 2.3 dB over the band of operation occurred in the third branch (the longest branch) which is expected. Errors in the phase remains constant for each branch.

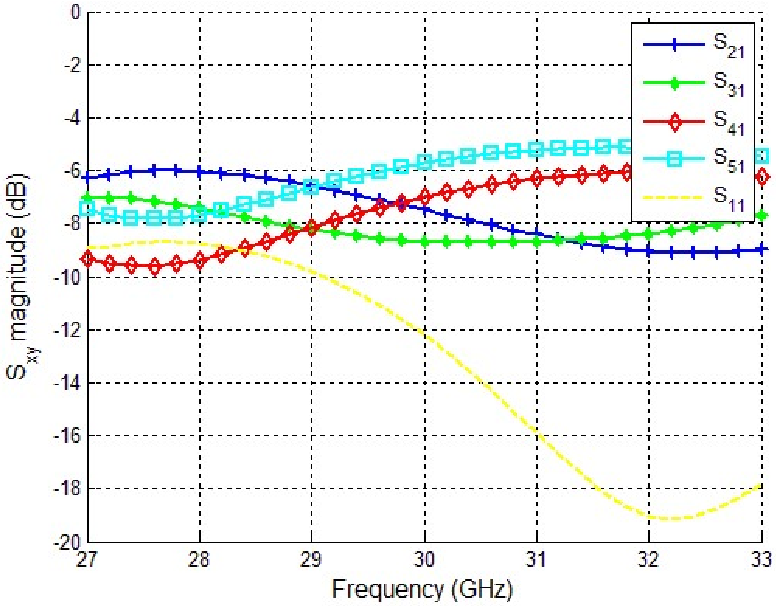

Figure 4.7: Feed Network $|S_{xy}|$

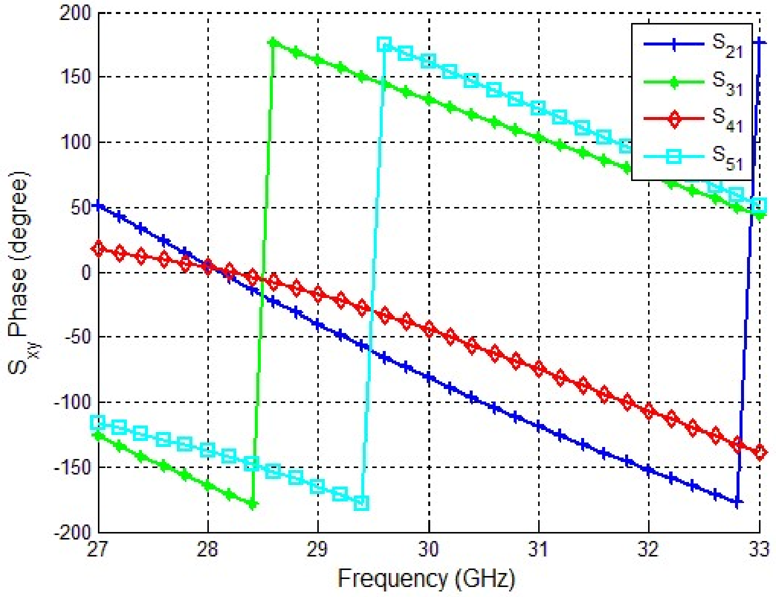

Figure 4.8: Feed Network Sxy (Phase)

4.5 Integration and Full Two-port MIMO Antenna System

To complete the design, the cDRA MIMO arrays and the feed network were combined as shown in Figure 4.9. The connector was also modeled to account for

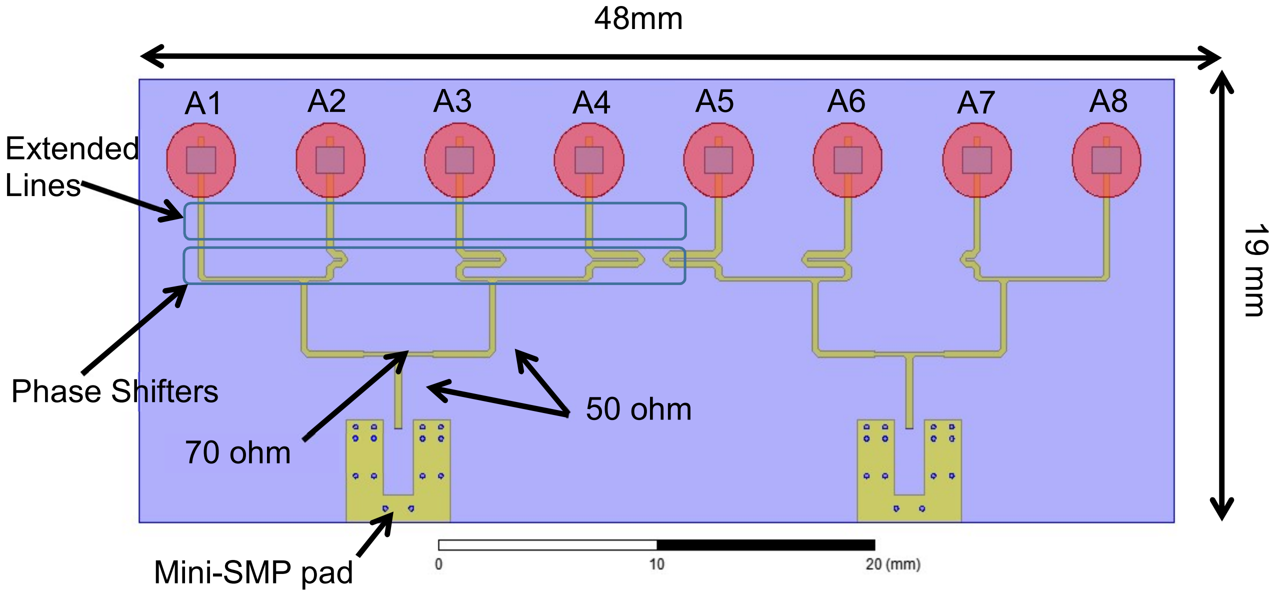

Figure 4.9: complete Design (cDRA + Feed Network)

fabrication effects in a later stage. The output lines from the network were extended by 3mm for impedance matching as shown in Figure 4.9.

Figure 4.10 shows the simulated reflection and isolation curves for the design. It was possible to achieve a bandwidth of 3 GHz around 29.5 GHz which is very desirable. Over the band of operation, isolation of at least 27 dB was maintained.

The envelop correlation coefficient (ECC) between the two ports is calculated from the simulated 3-D fields according to (37) for 29.5 GHz, 30 GHz and 30.5 GHz. Since the efficiency of the design is high (>90%), equation (38) is somehow valid. The correlation coefficient from the simulated S-parameters is calculated for the complete band of operation. Both ECC calculated values based on (37) and (38) are plotted in Figure 4.11. It is noted that –from both equations- the ECC did not exceed 0.0005 which implies excellent low correlation –and hence- good MIMO performance from the antenna system.

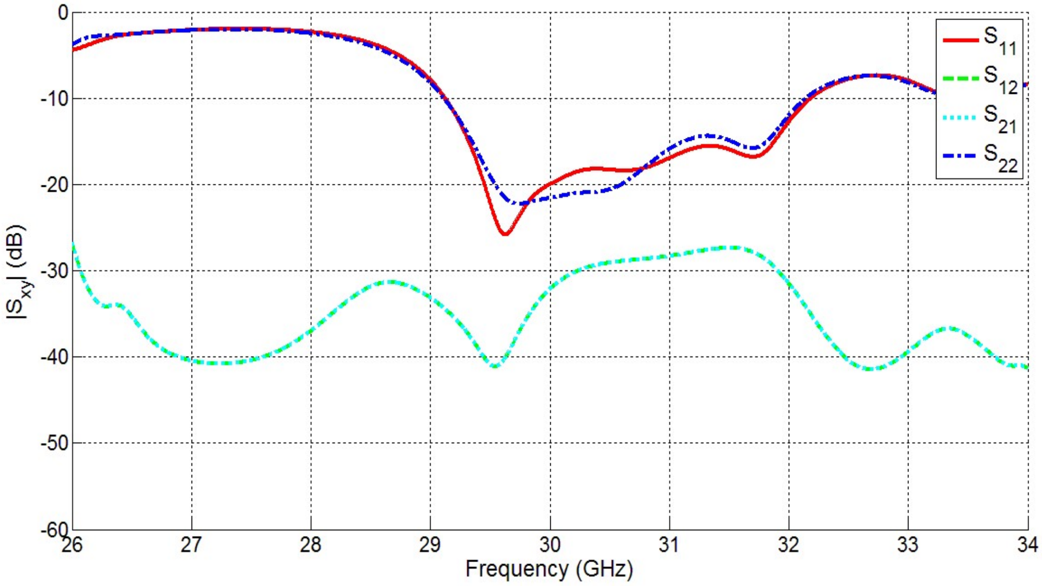

Figure 4.10: |Sxy| for the complete design

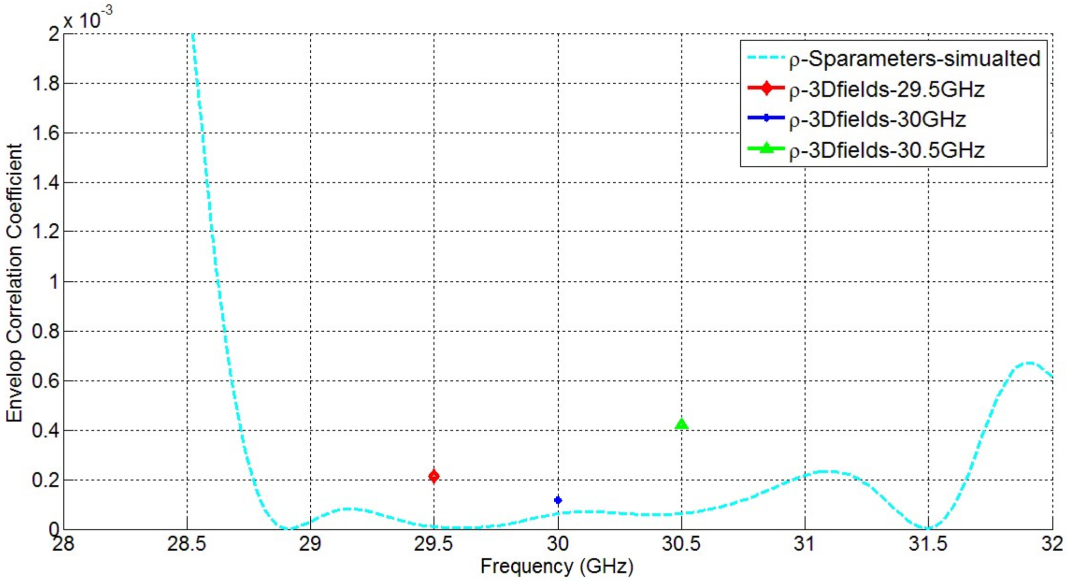

Figure 4.11: ECC from the simulated results between the two ports

4.6 Summary

A two-port MIMO antenna system operating at 30 GHz was designed. Each MIMO port was feeding four cDRA elements. The design started by designating the cDRA geometry through theoretical calculations and then validated and optimized using Full wave simulator. The design of a single cDRA was extended to construct the cDRA array and then the MIMO design. Next, a passive feed network was designed to feed the array cDRA elements with equal signals in magnitude with a progressive phase of 153°. This resulted in beam tilt of 45° with opposite direction around the azimuth for the MIMO arrays. The overall design size is 48 x 19 x 3.1 mm^3 The design maximum gain was 9 dBi with more than 90% efficiency. The design showed good MIMO performance with port isolation of less than -25 dB and ECC of less than 0.0005.

CHAPTER 5

MIMO ANTENNA SYSTEM FABRICATION AND MEASUREMENTS

In this chapter, the fabricated design of the MIMO antenna system designed in the previous chapter is described. Measurements and deviations from the simulations are discussed.

5.1 The Fabricated Design

The design in the previous chapter was fabricated as shown in Figure 5.1. As mentioned in the previous chapter, the system's substrate used was Rogers3003 with a thickness of 0.13mm only (flexible substrate). Hence, to be able to handle the board for measurements without bending it or damage it, a rigid backing material of thickness 0.9mm and ε_r of 4.0 was attached to the top layer (on top of the ground plane). The end of the backing material was at least 8mm from the cDRA elements. Figure 5.2 shows the modified model in HFSS after adding the supporting material to study its effects.

The cDRA elements were machined (cut) and glued to the PCB in Royal Military College (RMC) of Canada and assembled manually on the PCB. The PCB and the mini-SMP connectors attachment were conducted in Printech Labs, UK. A glue material with ε_r of 10 was used to attach the cDRAs to the PCB. The mini-SMP ports, which can operate in 30 GHz range according to its datasheet, were assembled on the bottom layer to as the input ports of the MIMO antenna system. The cDRAs were manually machined and resulted with a diameter of 3.05mm (theoretical diameter is 3.1mm) for antenna 1 to antenna 7 and 3.06 mm for antenna 8. Hence, a shift in the resonance frequency as well as different responses between the two ports are expected. The fabricarted model is shown in Figure 5.1.

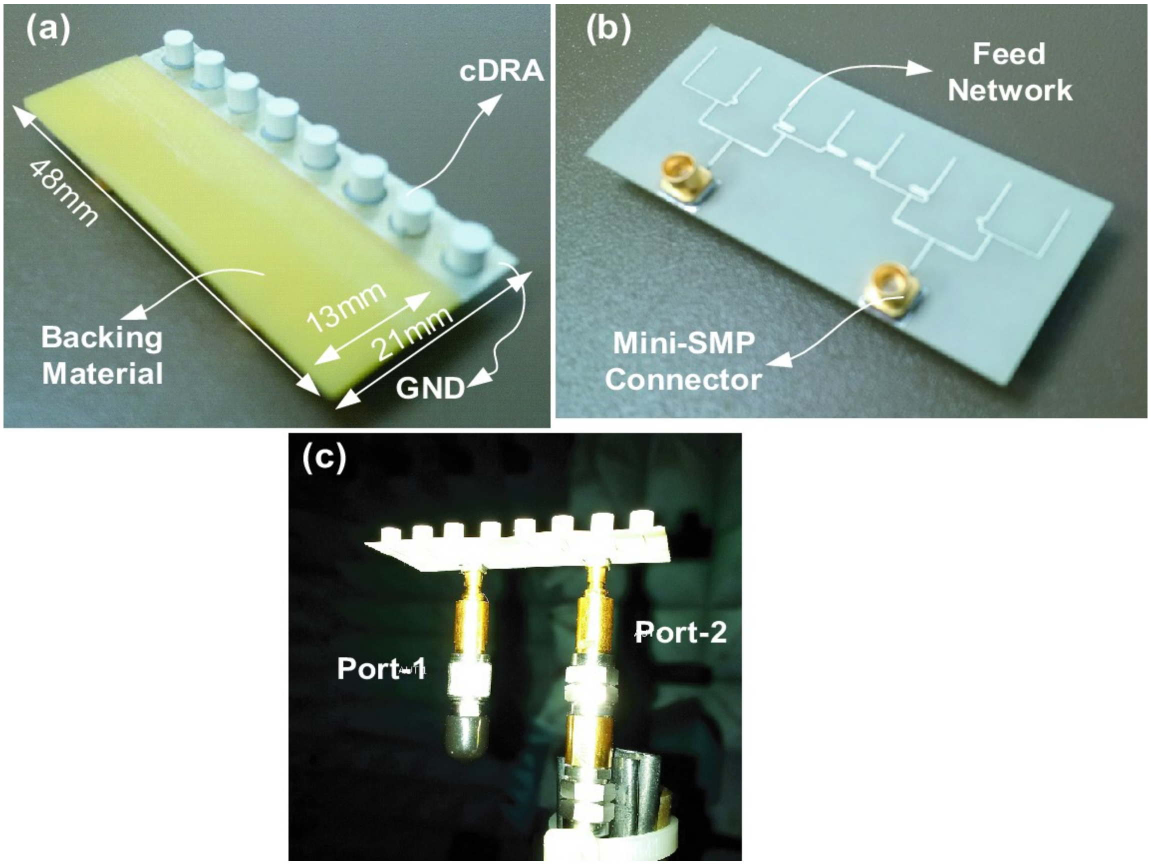

Figure 5.1: Fabricated model of the two-element cDRA array based MIMO antenna system (a) top view (b) bottom view (c) measurement setup

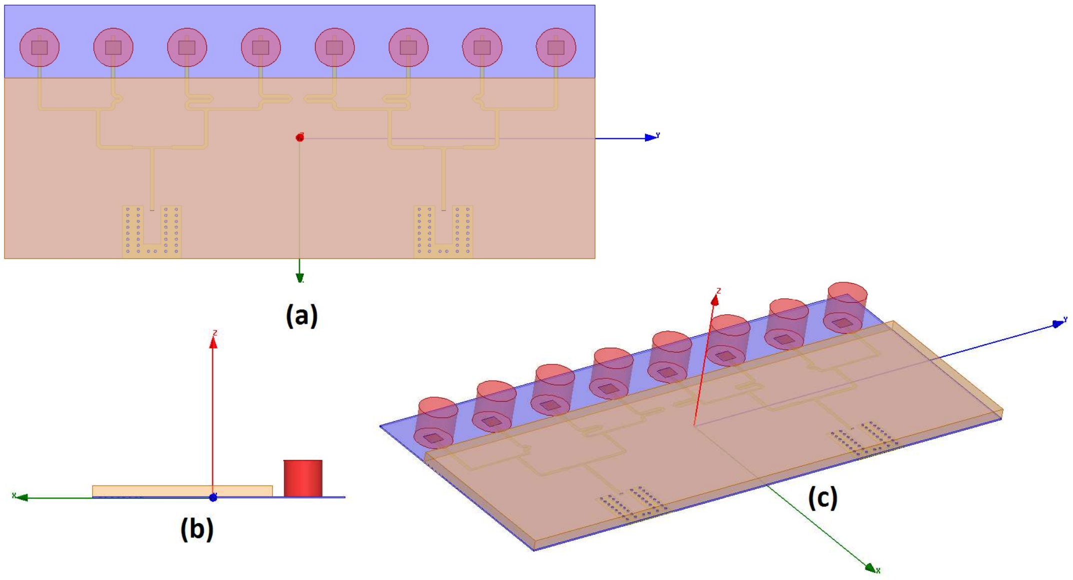

Figure 5.2: Fabricated model of the two-element cDRA array based MIMO antenna system (a) top view (b) bottom view (c) measurement setup

5.2 Measurements and Results

The readings of the S-parameters and 2-D radiation pattern were measured at Royal Military College (RMC), Canada. The readings are plotted here with the ideal case from simulation. Figure 5.3 shows the reflection coefficient response $|S_{xx}|$ of the ports of the system from the simulations and measurements. It can be noted that there is a shift in the resonance frequency of 2 GHz approximately for array 1. Array 2, on the other hand, experienced 0.5 GHz frequency shift.

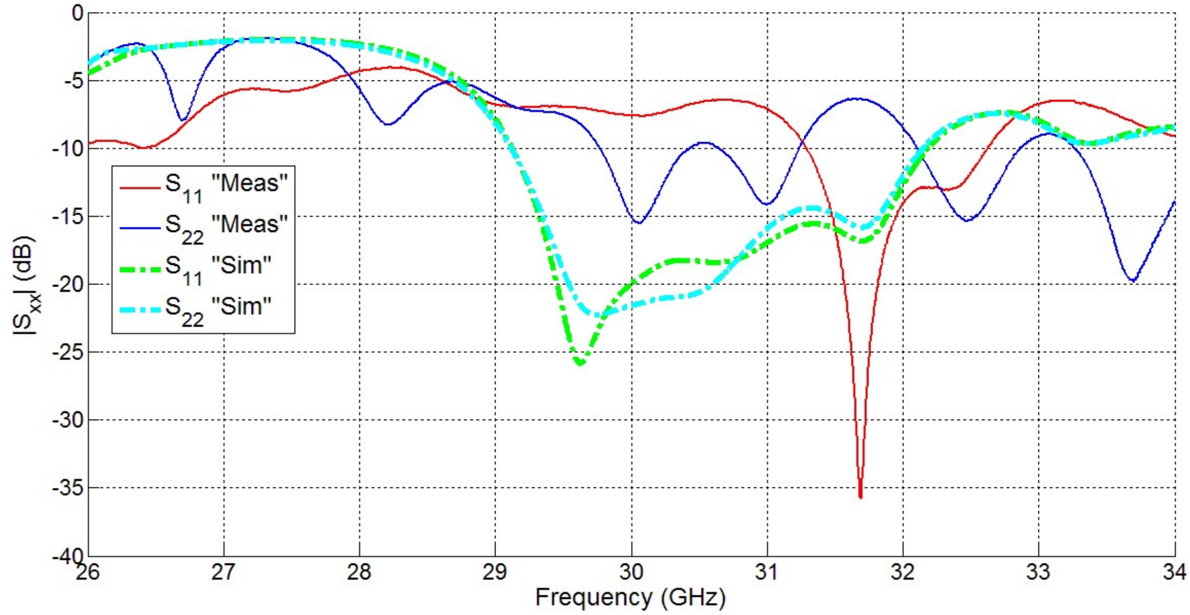

Figure 5.3: |Sxx| response “reflection coefficient” of the MIMO system (simulation and measurement)

Figure 5.4 shows the port coupling response from simulation and measurement. It is noted that good isolation between port (<-30 dB) was maintained. In Figure 5.5 and Figure 5.6, the measured 2D radiation patterns at 30 GHz and 31 GHz are shown respectively. (a) in both figures the pattern from the right array where (b) shows the pattern from the left array. A clear tilt towards 45 in the YZ-plane can be noted for both arrays in both figures. It also can be noted that the maximum gain is around 8 dBi. It can be also noted that the secondary lobe is less than the main lobe by at least 3 dB in all cases. This large side lobe level is expected to exist for relatively low number of antenna array elements which is 4 in our case. If the elements increased to 8, the lobe is expected to be have a smaller value. However, this will require doubling the feed network which will add additional degradation to the signal before reaching the antenna elements. Furthermore, the ripples seen in the measured 2D patterns can be related to the non-idealties in the measuring setup and environment.

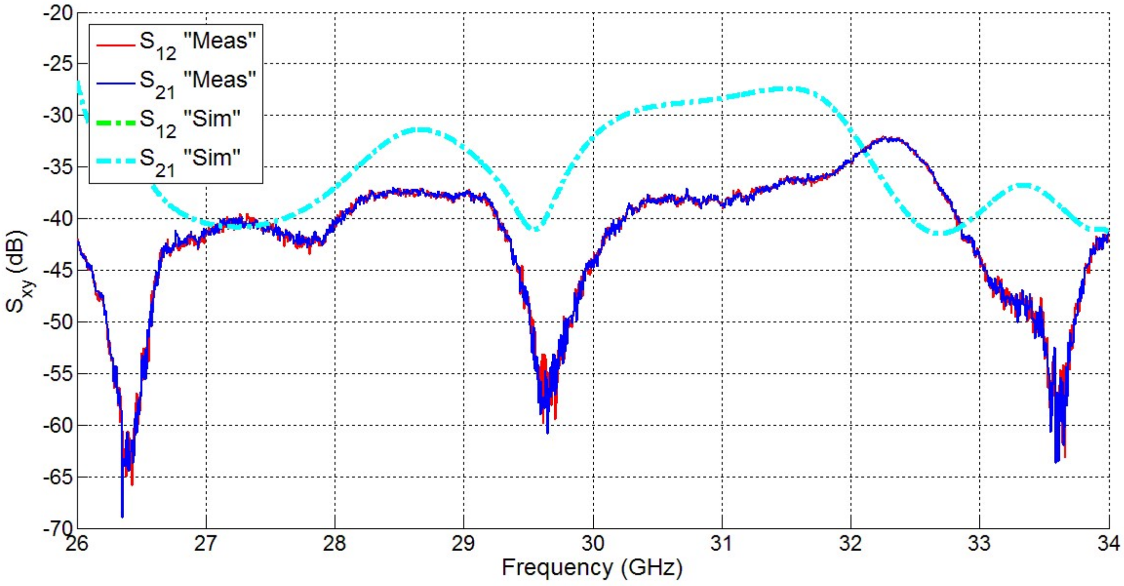

Figure 5.4: |Sxy| response of the MIMO system (simulation and measurement)

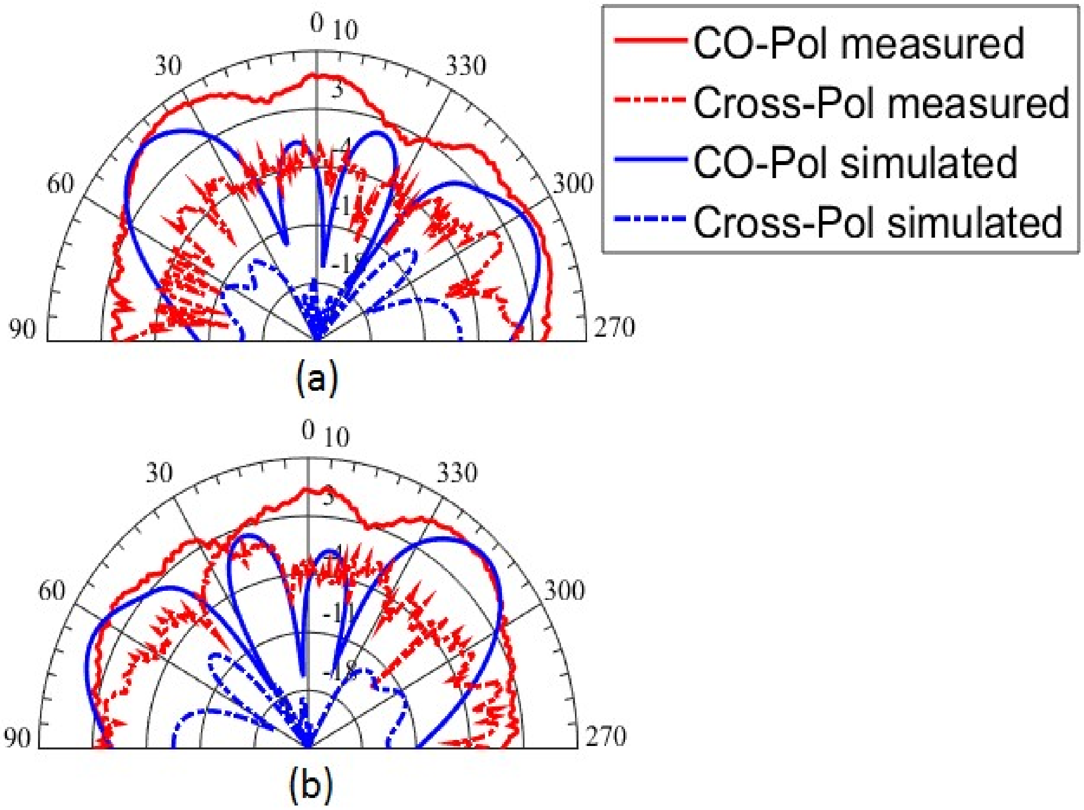

Figure 5.5: Measured 2D radiation patterns at 30 GHz (a) right array. (b) left array

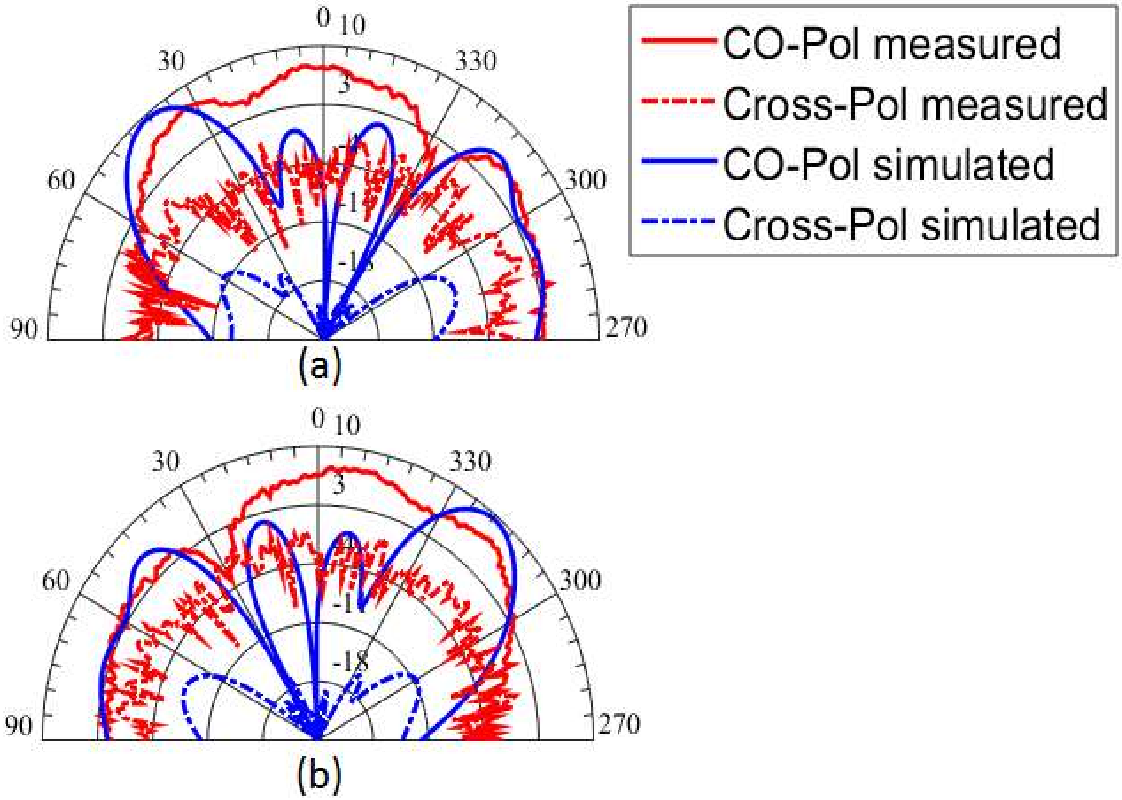

Figure 5.6: Measured 2D radiation patterns at 31 GHz (a) right array. (b) left array

To have a better visualization of the gain patterns, the normalized and filtered measured and simulated patterns were plotted for 30 GHz in Figure 5.7 and for 31 GHz in Figure 5.8. It can be noted the good match between simulation and fabrication despite manufactuing and material tolerances.

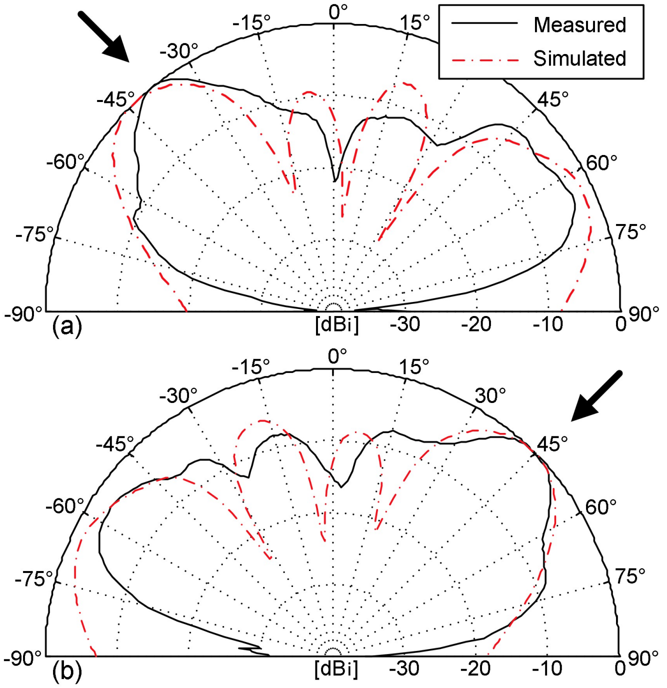

Figure 5.7: 2D radiation measured and simulated radiation patterns at 30 GHz (a) left array (b) right array

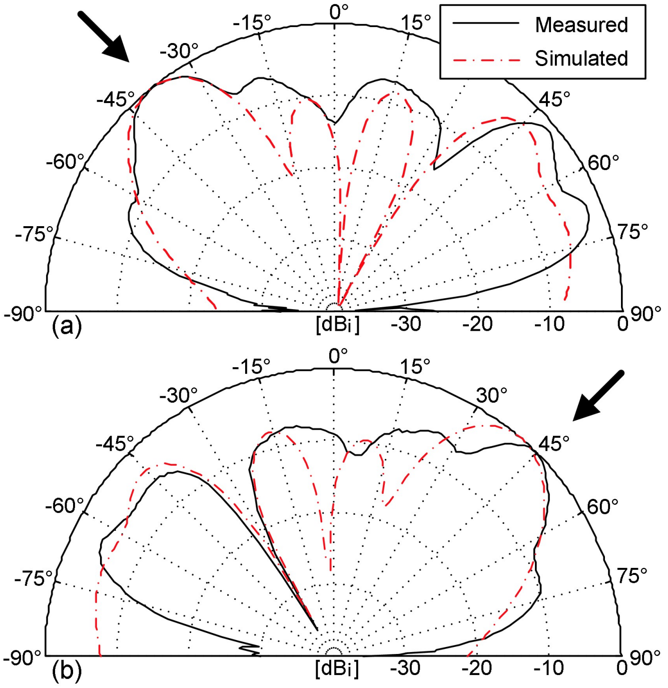

Figure 5.8: 2D radiation measured and simulated radiation patterns at 31 GHz (a) left array (b) right array

As there is a good match between simulated and measured radiation patterns, the envelop correlation coefficient obtained from the measured S-parameters and did not exceed 0.002 in the band of operation which is the case with the simulation results as well as shown in Figure 5.9.

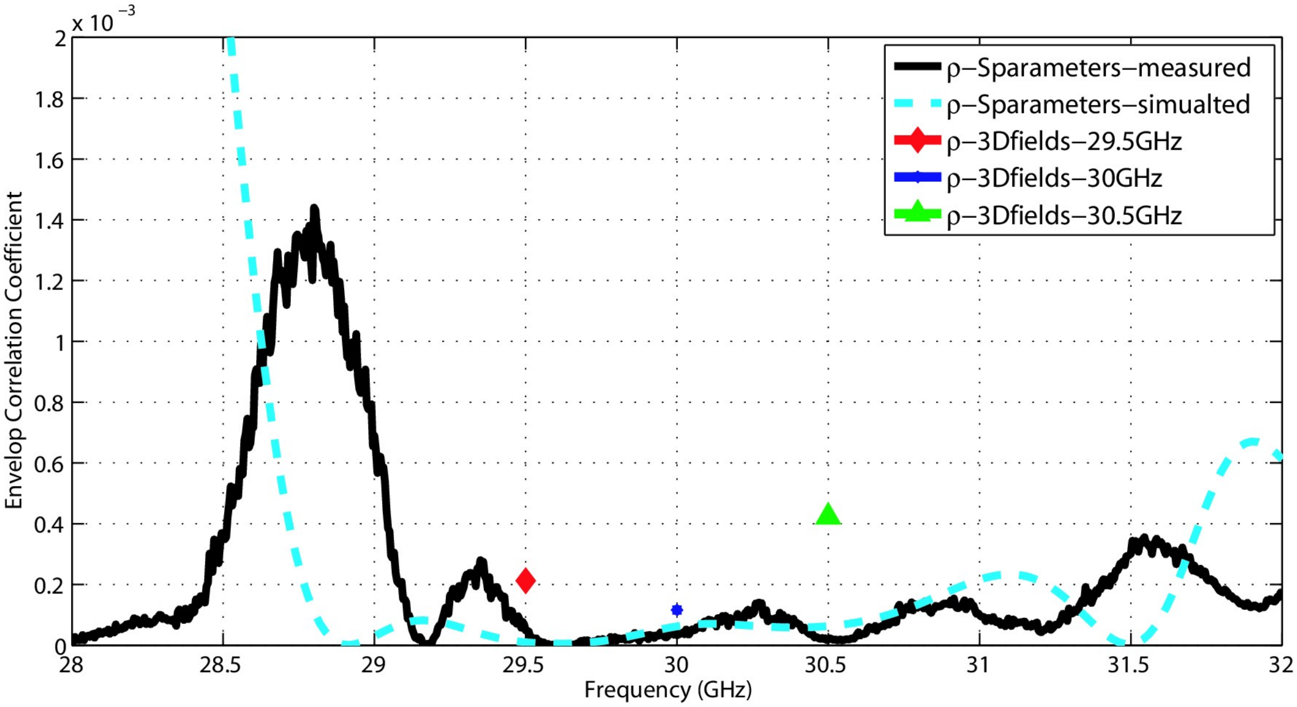

Figure 5.9: ECC for measured and simulated responses of the MIMO system

5.3 Parametric Studies

Several parametric studies were conducted in HFSS to investigate the effect of manufacturing and material tolerances.

5.3.1 Vertical Misalignment of the cDRA elements

Since the cDRAs were mounted on the board manually, a vertical and horizontal shift in the placement of the cDRA was noticed. Figure 5.10 shows the shift in resonance frequency if all cDRA elements were misplaced vertically by the same value (up or down) while they were centered horizontally (no shift to the left or right)

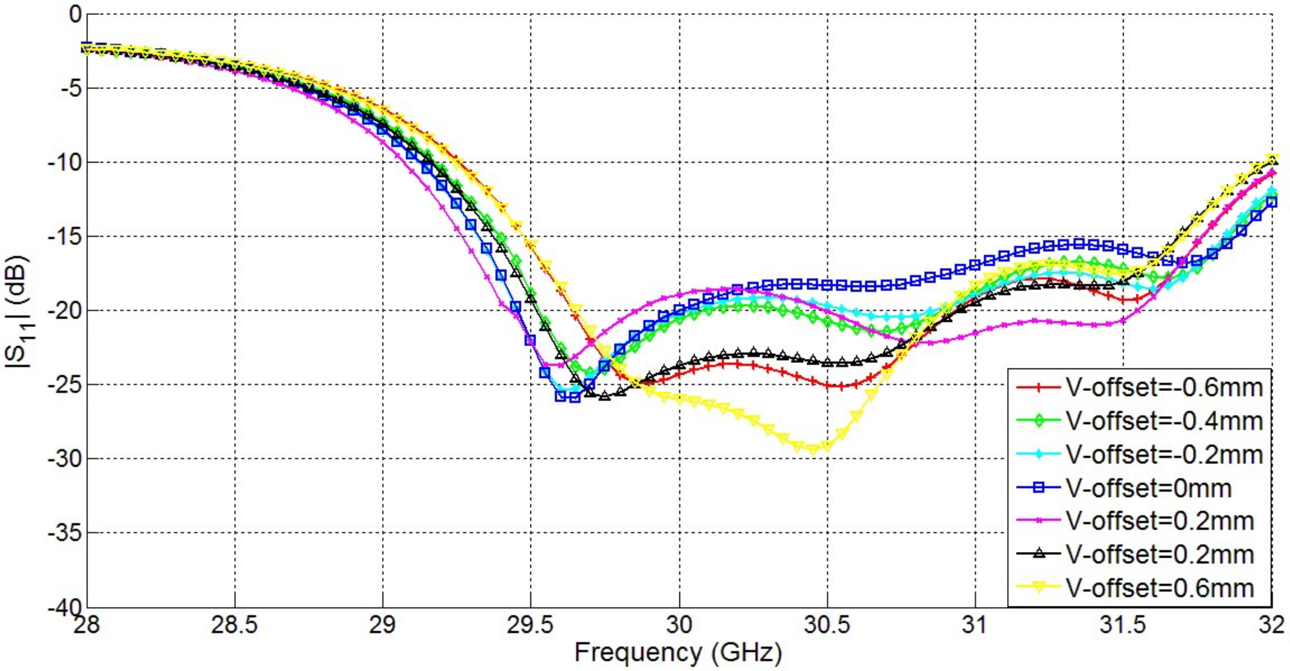

Figure 5.10: The effect of vertical shifts in the placement of the cDRA elements on the frequency

It is noted that the array experiences a shift in the resonance frequency by almost 1.6 GHz for a vertical shift of 0.6 mm upwards. Similarly, Figure 5.11 shows a shift in the of 1.7 GHz in the frequency with horizontal offset placement of the cDRA elements of 0.6mm to the left.

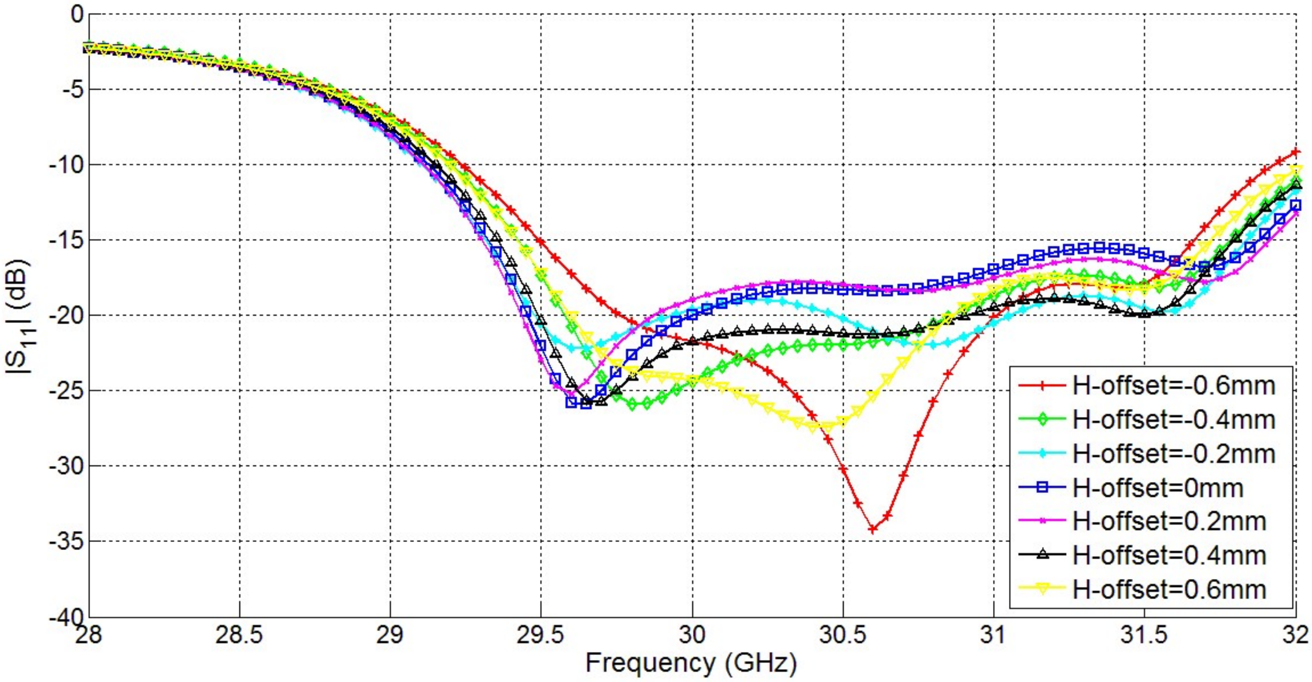

Figure 5.11: The effect of horizontal shifts in the placement of the cDRA elements on the frequency

Similar studies were conducted for extreme cases. In Figure 5.12, for example, horizontal shift was fixed at -0.6mm for (a) while the vertical shift is swept. In (b) horizontal shift was fixed at 0.6mm while the vertical shift is swept from -0.6 mm to 0.6mm. Similarly, in (c) the vertical shift was fixed at -0.6mm while the horizontal shift is swept while in (d) the vertical shift was fixed at 0.6mm while the horizontal shift is swept. All cases experienced a shift in the frequency from few hundred megahertz up to 1.7 GHz.

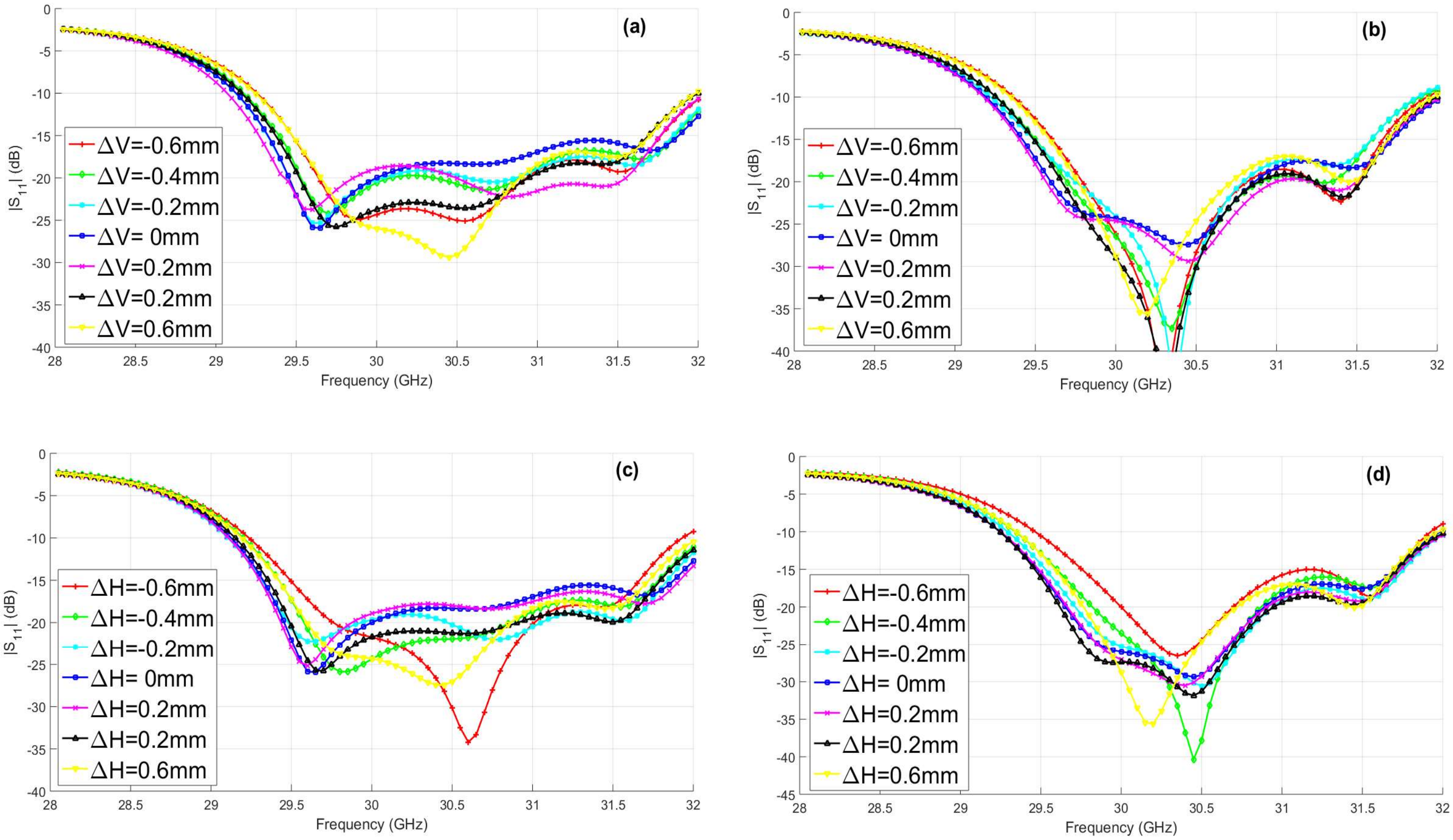

Figure 5.12: Extreme vertical and horizontal cDRA placement shifts (a) H_offset=-0.6mm (b) H_offset=0.6mm (c) V_offset=-0.6mm (d) V_offset=0.6mm

5.3.2 DRA Diameter

The diameter of all DRAs was swept from 3.0mm to 3.6mm (designed at 3.2mm). It can be seen the resonance frequency is shifted from 29.2 GHz (at 3.4mm) to 31.2 GHz (at 3.0mm) as shown in Figure 5.13.

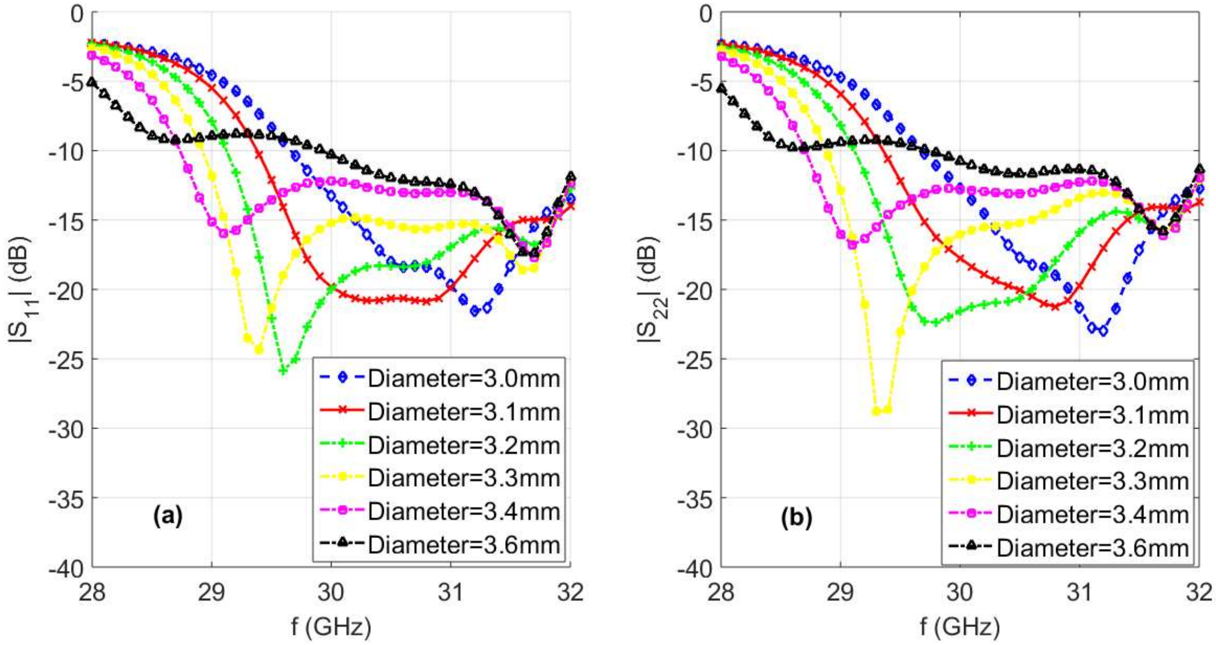

Figure 5.13 Effect of cDRA diameter manufacturing tolerances (Uniform sweep)

The diameter of the DRAs was swept in non-uniform way. In other words, the diameter of each DRA was changed by different value of other DRA. Values of variations varied among 3.0mm, 3.2mm and 3.4mm. Multiple resonance frequencies appeared since every DRA is resonating in a different frequency as shown in Figure 5.14. It can be noticed that the combination (3.2,3.2,3.4,3.4) which is solid yellow has a similar response to the measured S22 response

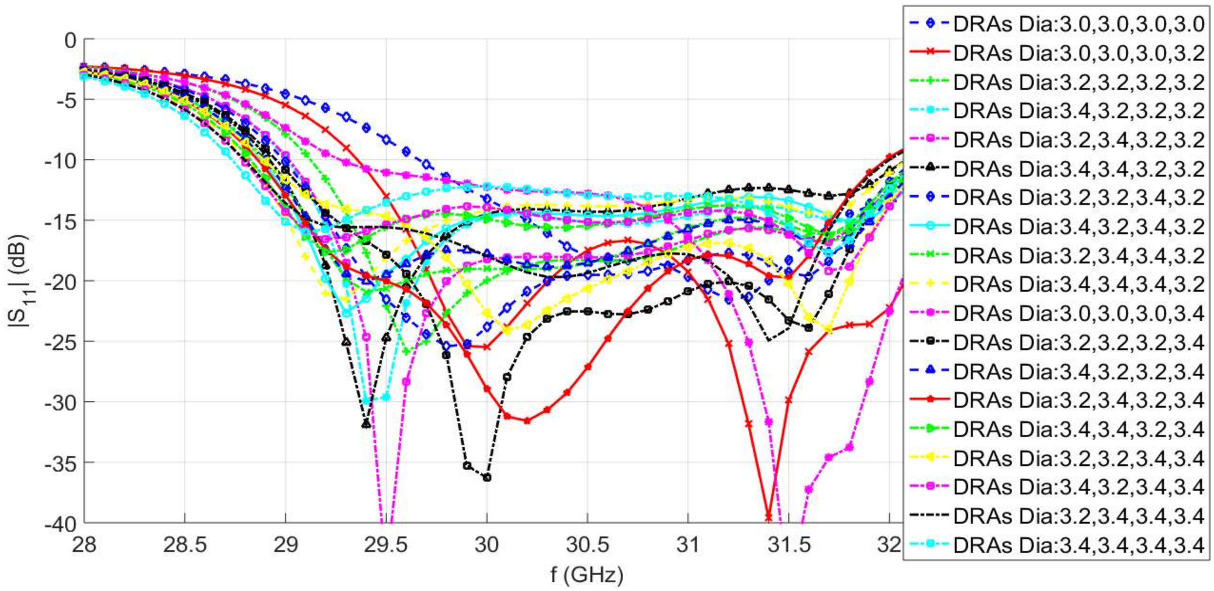

Figure 5.14 Effect of cDRA diameter manufacturing tolerances (Ununiformed sweep)

5.3.3 DRA dielectric constant

The dielectric constant of the DRA was swept from 9.8 to 10.4. It can be seen the resonance frequency is inversely proportional to ε_r. As shown in Figure 5.15 for both MIMO arrays, where (a) shows the reflection coefficient curves of left array and (b) shows the reflection coefficient curves of the right array, the resonance frequency is shifted 1.5 GHz from 29.2 GHz to 30.7 GHz.

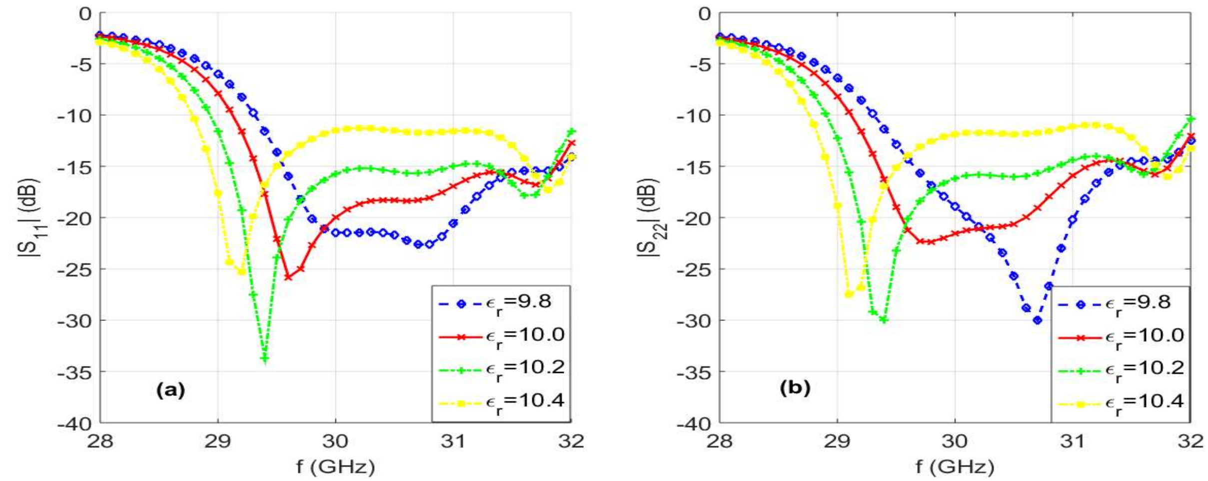

Figure 5.15 Effect of cDRA material tolerance (ε_r)

5.3.4 Additional height

The height of the DRA was increased from 0mm to 0.1mm in 0.02mm steps. It can be seen in Figure 5.16 that there is a slight shift in the resonance frequency due to change in cDRA height.

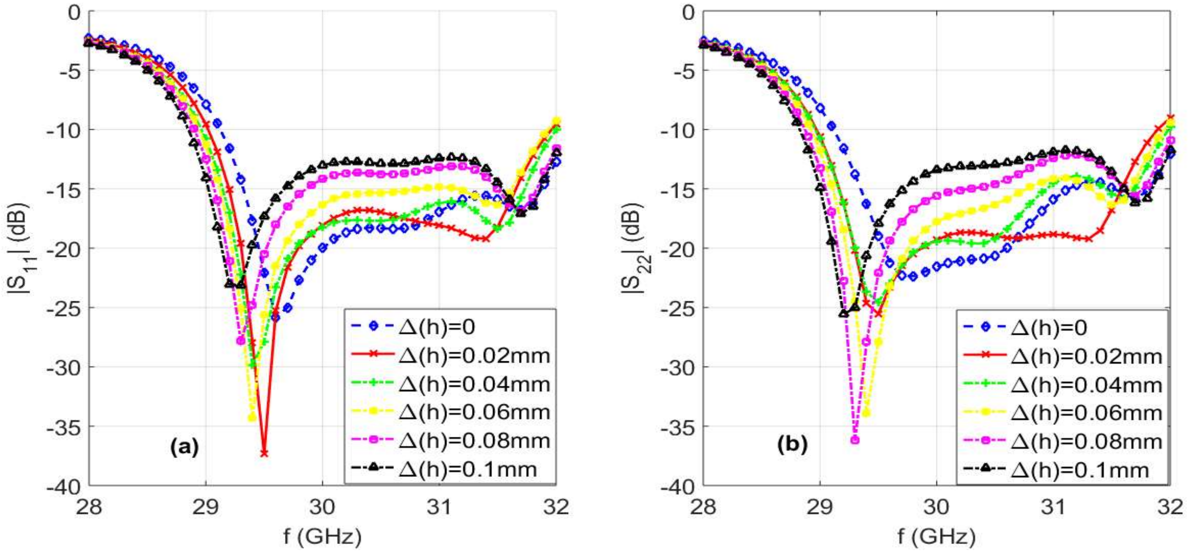

Figure 5.16 Effect of cDRA manufacturing tolerance (height)

It is worth noting that this study includes the effect of additional height due to manufacturing error as well as the additional height caused by the bonding agent (glue).

5.3.5 DRA loss tangent

The loss tangent of the DRA material was swept from 0.002 to 0.014. It can be seen the resonance frequency is directly proportional to the loss tangent. A Shift of almost 1 GHz was observed.

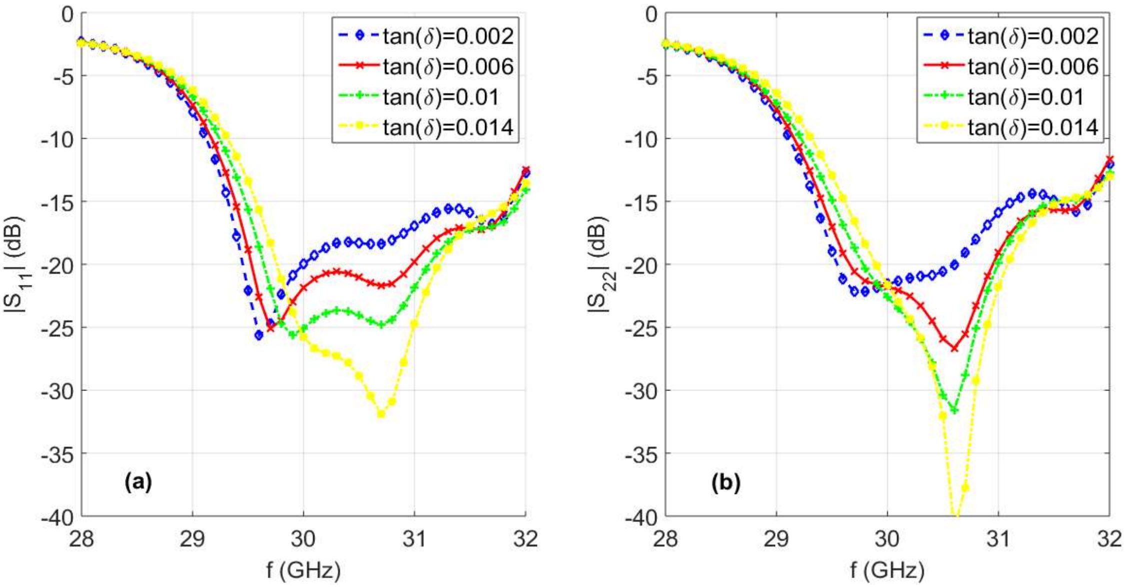

Figure 5.17 Effect of cDRA material tolerance (loss tangent)

A special case where the effects DRA dielectric constant (-2% variation) as well as the addition of the height of 0.1 mm due to the bonding agent were incorporated in S_{xx} Sim-eff curve in Figure 5.18. It shows a good agreement in the 10 dB bandwidth with measured values (S_{xx}-Meas) curve as shown in the figure. Other discrepancies in S_{xx} curves are resulted from fabrication tolerances as shown in the parametric studies.

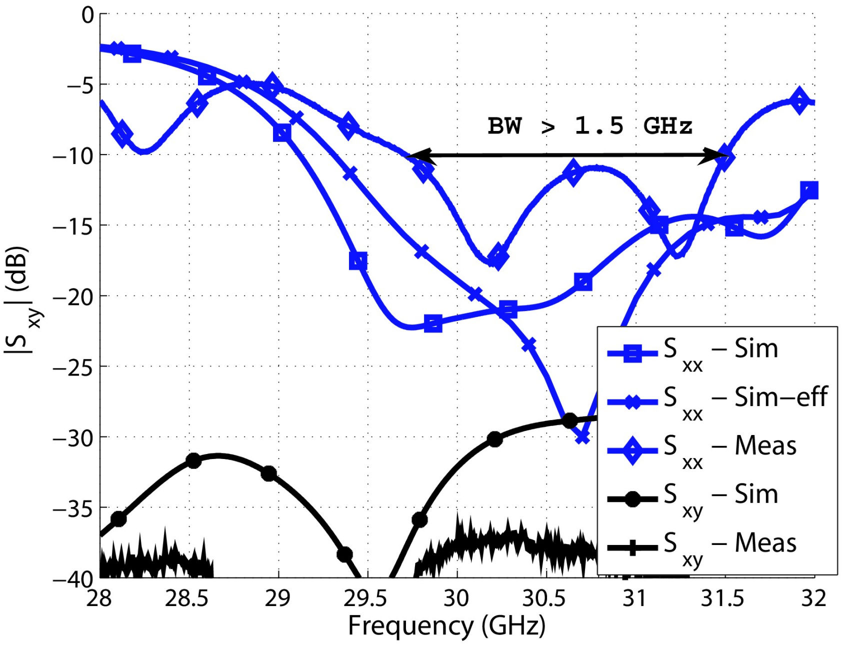

Figure 5.18: Measured and simulated S-parameters for the mm-wave cDRA based MIMO antenna system

MIMO antenna system

5.4 Summary

The two-port MIMO cDRA array based antenna system designed in the previous chapter was fabricated and analyzed. The fabricated system showed good match with simulation in terms of maximum gain, radiation pattern and MIMO performance. A shift in the resonance frequency in the fabricated model was noted due to manufacturing tolerances and material non-idealities. Several parametric studies were conducted to characterize the causes of the shift. Non-uniform changes in cDRA diameter was noticed to have a major effect in the shift and S-parameter response disturbance which was also seen the reflection coefficient response of the second array in the fabricated design. The increase in the diameter is due to the glue material as well as manufacturing tolerances.

CHAPTER 6

EXPANDING THE DESIGN

6.1 Four port MIMO System

The design in section 4.4 was taken a step further to support a 4 port MIMO configuration. A 4-port MIMO array is proposed and modeled based on the 4-element linear cDRA configuration. For compactness, each two arrays with opposite radiation patterns are placed against each other as depicted in Figure 6.1. The distance between opposite cDRAs are kept at 6mm. The complete design is fitted in area of 72x39 mm^2 of a system substrate of thickness 0.13mm. Only simulation results are provided as this design is not fabricated.

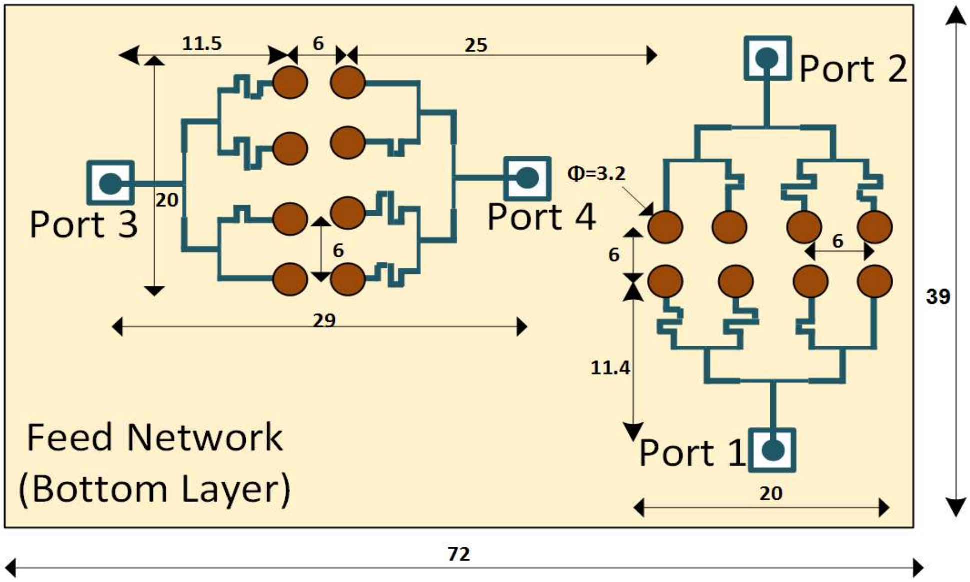

Figure 6.1: Schematics of the 4x4 MIMO Design

Figure 6.2 shows the reflection coefficient curves $|S_{xx}|$ while Figure 6.3 shows the isolation curves $|S_{xy}|$ between the four ports. 15 dB of isolation was maintained which is acceptable. The lowest isolation occurred between opposite arrays.

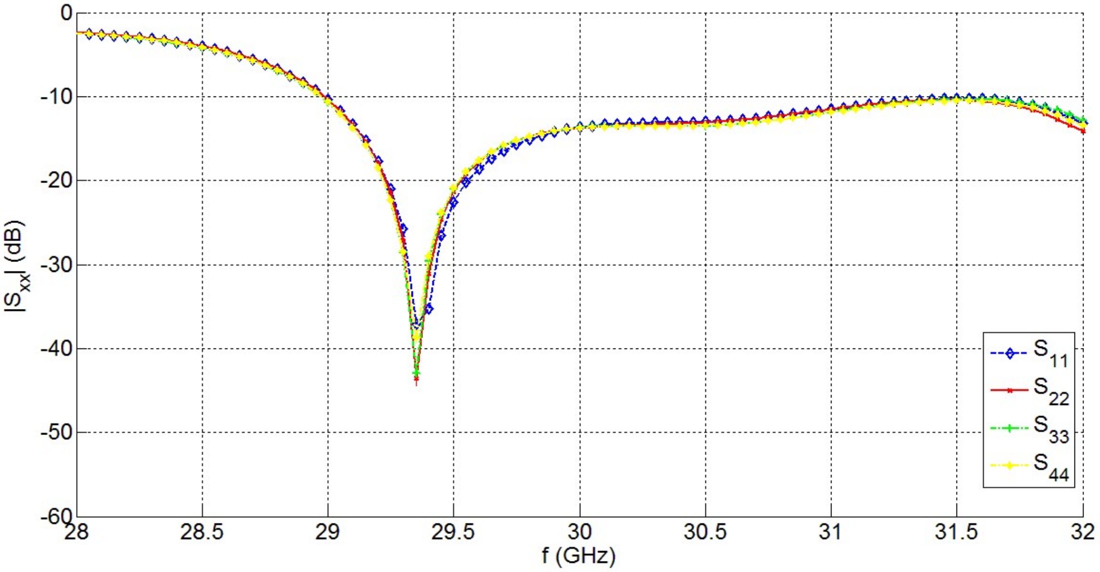

Figure 6.2: |Sxx| for the 4x4 MIMO Array

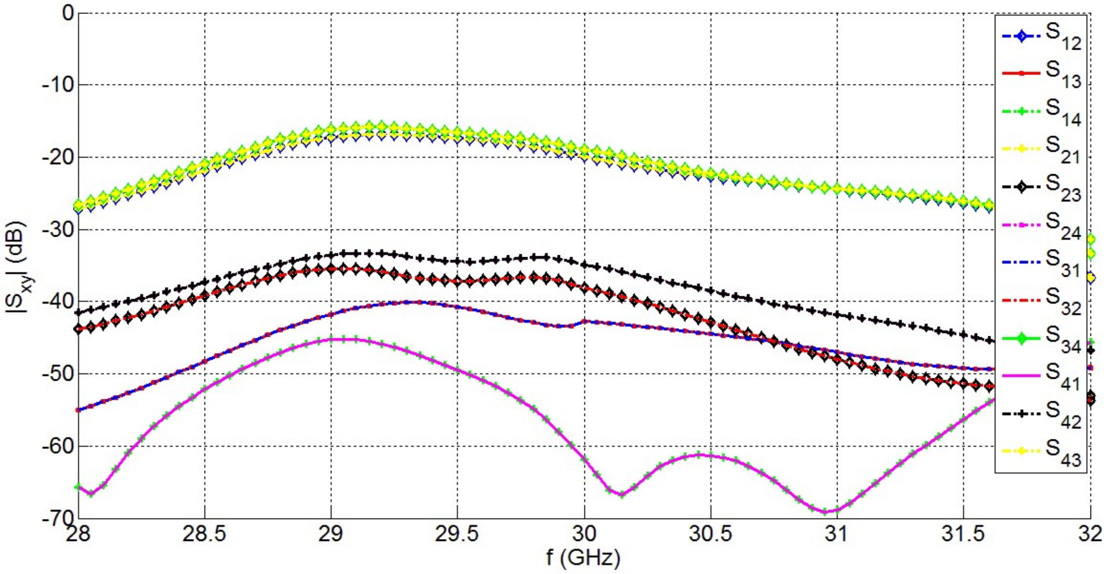

Figure 6.3: |Sxy| for the 4x4 MIMO Array

The radiation patterns for the four arrays are shown Figure 6.4. The maximum gain was found to be 10 dBi. The beams are tilted in a unique direction for each port as required for good MIMO operation. From the simulated radiated fields and from the S-Parameters, the Envelop Correlation Coefficient is calculated and plotted in Figure 6.5. The maximum ECC did not exceed 0.01.

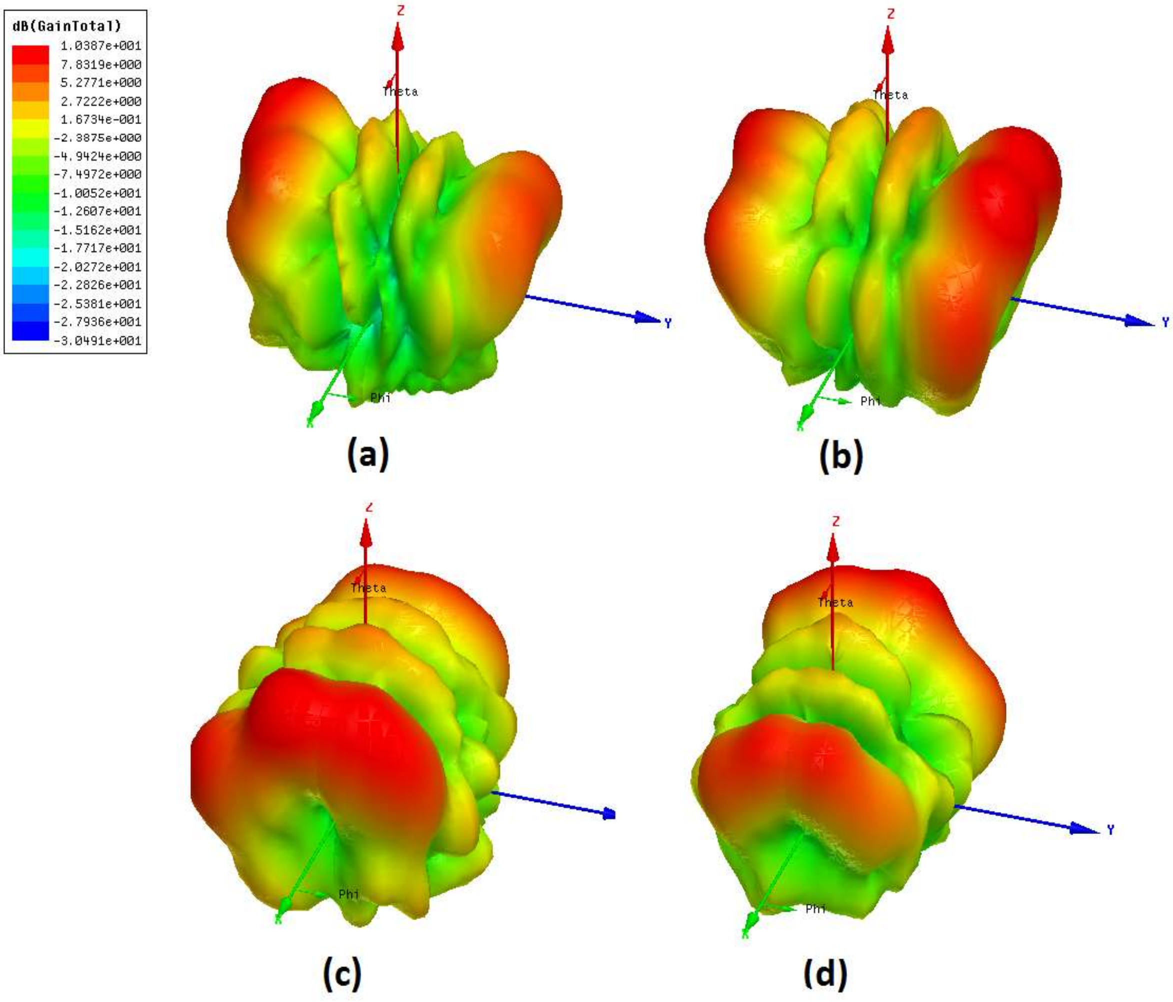

Figure 6.4: simulated radiation patterns for the MIMO structure (a) for array 2, (b) for array 1, (C) for array 3 and (D) for array 4.

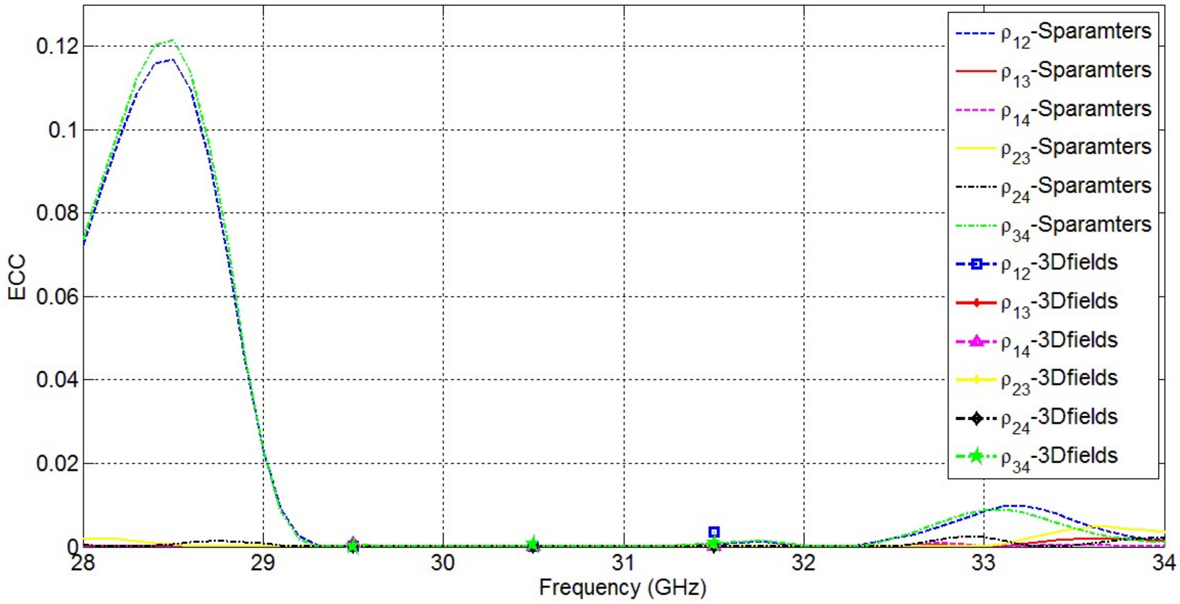

Figure 6.5: Correlation Coefficient (ρe) values between the four array obtained from the simulated S-Parameters and 3-D fields

6.2 Summary

To enhance the channel capacity, a four-port MIMO cDRA array based antenna system was designed. The design was based on the previous 2-port MIMO antenna system. To improve the system compactness, the arrays were arranged in opposite directions. However, this was on the expense of the MIMO performance where the worst isolation between ports was found to be at -15 dB and ECC was below 0.01 (compared to -25 dB and 0.002 from the 2-port design). However, this is still considered good MIMO performance. The overall design occupied a volume of 72 x 39 x 3.1mm^3 and had a maximum gain of 10 dBi.

CHAPTER 7

CONCLUSION AND FUTURE WORK

7.1 Conclusions

In this work, MIMO cDRA-based antenna systems for the 5G standard are investigated. Due to its numerous advantages, MIMO is a vital enabling technology in the upcoming 5G standard. Not only that, since the 5G is intending to use the mm-wave range of the spectrum, it is essential to utilize antenna elements that are of high efficiency and gain. This is where dielectric resonator antennas (DRAs) become a viable option to design mm-wave antennas due to the absence of metallic losses. Despite their 3D structures which is not preferable in printed circuit technology, their size in the mm-wave range becomes negligible. Combining MIMO and DRAs is expected to provide a state-of-the-art solution for future 5G designs.

Multiple configurations for MIMO cylindrical-DRA-based antenna systems are designed. All consist of a basic array of cDRA elements. The cDRA are fed with a passive network that provides predefined phases inputted to the cDRA elements that results in a fixed beam tilt. Two linear arrays are used to design a 2 port MIMO system. The system occupied an area of 48x21mm^2. Simulation results showed a maximum gain of 9 dBi with efficiency above 90%. 3D radiation patterns showed clear beam tilts of 45 degrees in opposite directions around the azimuth which resulted in envelop correlation coefficient (ECC) of less than 0.002 which indicated good MIMO behavior. Fabrication results showed a maximum gain of 8 dBi. Good match between the measured radiation pattern and simulated one.

Some discrepancies for the reflection coefficient response were observed between the simulation and measurements. The first array showed a shift in the center frequency of 1.5 GHz approximately while the second array showed multiple resonances. For that, a thorough parametric analyses were conducted to characterize these differences. Both human and machining errors were taken into consideration as well material non-idealities. The parameters that were investigated included: DRA misplacement, change in DRA diameter, height, dielectric constant and loss tangent where two percent errors introduced for each case. The most contributing parameters found for the frequency shift are the DRA misplacement and DRA diameters errors.

A compact design of four port MIMO systems was designed based on the previous configuration. However, each 2 arrays are opposite to each other but still radiating in opposite directions. The simulated maximum gain was 10 dBi while the ECC did not 0.01 and isolation between the ports was below -15 dB. The system occupied an area of 72x39 mm^2. The two proposed designs can fit easily within the edges of future mobile devices.

7.2 Future Work

This work can be extended in the future by using an active feed network. The active feed network can tilt the beam to obtain the best isolation and lowest correlation. Reduction of the size of the feed network can be also investigated which will lead to a significant reduction of the overall system size. Furthermore, an ultra-wide band DRA can be integrated with the design for the purpose of spectrum sensing. Together, an advanced solution for 5G communication systems can be proposed.

REFERENCES

[1] N. Kroes, "Press releases database, European Commission.," 24 February 2014. [Online]. Available: http://europa.eu/rapid/press-release_MEMO-14-129_en.htm. [Accessed 17 November 2015].

[2] F. J. Escribano, "An overview on current trends in mobile communications," 7 July 2015. [Online]. Available: http://www.slideshare.net/FranJEscribano/an-overview-on-current-trends-in-mobile-communications. [Accessed 17 November 2015].

[3] M. S. Sharawi, Printed MIMO Antenna Engineeering, Artech House, 2014.

[4] M. S. Sharawi, "Printed Multi-Band MIMO Antenna Systems and Their Performance Metrics," *IEEE Antennas and Propagation Magazine,* vol. 55, no. 5, pp. 218-232, October 2013.

[5] A. Petosa, Dielectric Resonator Antenna Handbook, Artech House, 2007.

[6] R. K. Mongia and P. Bhartia, "Dielectric Resonator Antennas: A Review and General Design Relations for Resonant Frequency and Bandwidth," *International Journal on RF and Micowave Computer Aided Engineering ,* vol. 4, no. 3, pp. 230-247, 1994.

[7] K. M. Luk and K. W. Leung, Dielectric Resonator Antennas, Research Studies Press, 2003.

[8] C. A. Balanis, Antenna Theory: Analysis and Design, Wiley-Interscience, 2005.

[9] D. M. Pozar, Micowave Engineering, Wiley, 2005.

[10] L. Zou, D. Abbott and C. Fumeaux, "Omnidirectional Cylindrical Dielectric Resonator Antenna With Dual Polarization," *IEEE Antennas and Wireless Propagation Letters,* vol. 11, pp. 515-518, 2012.

[11] D. Guha, A. Banerjee, C. Kumar and Y. Antar, "New Technique to Excite Higher-Order Radiating Mode in a Cylindrical Dielectric Resonator Antenna," *IEEE Antennas and Wireless Propagation Letters,* vol. 14, pp. 15 - 18, 2014.

[12] N. Yang, K. W. Leung and E. H. Lim, "Mirror-Integrated Dielectric Resonator Antenna," *IEEE Transactions on Antennas and Propagation,* vol. 62, no. 1, pp. 27-32, 2014.

[13] S. Fakhte, H. Oraizi and R. Karimian, "A Novel Low-Cost Circularly Polarized Rotated Stacked Dielectric Resonator Antenna," *IEEE Antennas and Wireless Propagation Letters,* vol. 13, pp. 722-725, 2014.

[14] M. Khalily, M. Kamarudin, M. Mokayef and M. Jamaluddin, "Omnidirectional Circularly Polarized Dielectric Resonator Antenna for 5.2-GHz WLAN Applications," *IEEE Antennas Wireless and Propagation Letters,* vol. 13, pp. 443-446, 2014.

[15] D. Hou, W. Hong, W.-L. Goh, J. Chen, Y.-Z. Xiong, S. Hu and M. Madihian, "D-band on-chip higher-order-mode dielectric-resonator antennas fed by half-mode cavity in CMOS technology," *IEEE Antennas and Propagation Magazine,* vol. 56, no. 3, pp. 80-89, 2014.

[16] L. Ohlsson, T. Bryllert, C. Gustafson, D. Sjoberg, M. Egard, M. Arlelid and L. Wernersson, "Slot-Coupled Millimeter-Wave Dielectric Resonator Antenna for High-Efficiency Monolithic Integration," *IEEE Transaction on Antennas and Propagation,* vol. 61, no. 4, pp. 1599-1607, 2013.

[17] M. Al-Hasan, T. Denidni and A. Sebak, "Millimeter-Wave EBG-Based Aperture-Coupled Dielectric Resonator Antenna," *IEEE Transactions on Antennas and Propagation,* vol. 61, no. 8, pp. 4354-4357, 2013.

[18] X. Fang, K. W. Leung and E. H. Lim, "Singly-Fed Dual-Band Circularly Polarized Dielectric Resonator Antenna," *IEEE Antennas and Wireless Propagation Letters,* vol. 13, pp. 995 - 998, 2014.

[19] Y. M. Pan, S. Y. Zheng and B. J. Hu, "Design of Dual-Band Omnidirectional Cylindrical Dielectric Resonator Antenna," *IEEE Antennas and Wireless Propagation Letters,* vol. 13, pp. 710-713, 2014.

[20] Y. M. Pan, S. Y. Zheng and W. Li, "Dual-Band and Dual-Sense Omnidirectional Circularly Polarized Antenna," *IEEE Antennas and Wirless Propagation Letters,* vol. 13, pp. 706 - 709, 2014.

[21] M. Zhang, B. Li and X. Lv, "Cross-Slot-Coupled Wide Dual-Band Circularly Polarized Rectangular Dielectric Resonator Antenna," *IEEE Antennas and Wireless Propagation Letters,* vol. 13, pp. 532-535, 2014.

[22] O. Avadanei, M. Banciu and L. Nedelcu, "Higher-Order Modes in High-Permittivity Cylindrical Dielectric Resonator Antenna Excited by an Off-Centered Rectangular Slot," *IEEE Antennas and Wireless Propagation Letters,* vol. 13, pp. 1585-1588, 2014.

[23] Y. F. Wang, T. Denidni, Q. S. Zeng and G. Wei, "Band-notched UWB rectangular dielectric resonator antenna," *Electronics Letters ,* vol. 50, no. 7, pp. 483-484, 2014.

[24] A. Majeed, A. Abdullah, F. Elmegri, K. Sayidmarie, R. Abd-Alhameed and J. Noras, "Aperture-Coupled Asymmetric Dielectric Resonators Antenna for Wideband Applications," *IEEE Antennas and Wireless Propagation Letters,* vol. 13, pp. 927 - 930, 2014.

[25] Y. Wang, N. Wang, T. Denidni, Q. Zeng and G. Wei, "Integrated Ultrawideband/Narrowband Rectangular Dielectric Resonator Antenna for Cognitive Radio," *IEEE Antennas and Wireless Propagation Letters,* vol. 13, pp. 694-697, 2014.

[26] I. Messaoudene, T. Denidni and A. Benghalia, "Ultra-wideband DRA integrated with narrow-band slot antenna," *Electronics Letters,* vol. 50, no. 3, pp. 139-141, 2014.

[27] M. Zou and J. Pan, "Wideband hybrid circularly polarised rectangular dielectric resonator antenna excited by modified cross-slot," *Electronics Letters ,* vol. 50, no. 16, pp. 1123-1125, 2014.

[28] X. S. Fang and K. W. Leung, "Design of Wideband Omnidirectional Two-Layer Transparent Hemispherical Dielectric Resonator Antenna," *IEEE Transactions on Antennas and Propagation,* vol. 62, no. 10, pp. 5353-5357, 2014.

[29] B. Mukherjee, P. Patel and J. Mukherjee, "A Novel Cup-Shaped Inverted Hemispherical Dielectric Resonator Antenna for Wideband Applications," *IEEE Antennas and Wireless Propagation Letters,* vol. 12, pp. 1240- 1243, 2013.

[30] C. Ozzaim, F. Ustuner and N. Tarim, "Stacked Conical Ring Dielectric Resonator Antenna Excited by a Monopole for Improved Ultrawide Bandwidth," *IEEE Transaction on Antennas and Propagation,* vol. 61, no. 3, pp. 1435-1438, 2013.

[31] M. Khalily, M. Kamarudin and M. Jamaluddin, "A Novel Square Dielectric Resonator Antenna With Two Unequal Inclined Slits for Wideband Circular Polarization," *IEEE Antennas and Wireless Propagation Letters,* vol. 12, pp. 1256-1259, 2013.

[32] R. Chaudhary, R. Kumar and K. Srivastava, "Wideband Ring Dielectric Resonator Antenna With Annular-Shaped Microstrip Feed," *IEEE Antennas and Wireless Propagation Letters,* vol. 12, pp. 595-598, 2013.

[33] X. S. Fang, K. W. Leung and K. M. Luk, "Theory and Experiment of Three-Port Polarization-Diversity Cylindrical Dielectric Resonator Antenna," *IEEE Transactions on Antennas and Propagation,* vol. 62, no. 10, pp. 4945- 4951, 2014.

[34] W. W. Li and K. W. Leung, "Omnidirectional Circularly Polarized Dielectric Resonator Antenna With Top-Loaded Alford Loop for Pattern Diversity Design," *IEEE Transactions on Antennas and Propagation,* vol. 61, no. 8, pp. 4246-4256, 2013.

[35] T. Apperley and M. Okoniewski, "An Air-Gap-Based Frequency Switching Method for the Dielectric Resonator Antenna," *IEEE Antennas and Wireless Propagation Letters,* vol. 13, pp. 455-458, 2014.

[36] J. Desjardins, D. McNamara, S. Thirakoune and A. Petosa, "Electronically Frequency-Reconfigurable Rectangular Dielectric Resonator Antennas," *IEEE Transactions on Antennas and Propagations,* vol. 60, no. 6, pp. 2997-3002, 2013.

[37] W. Abdel-Wahab, D. Busuioc and S. Safavi-Naeini, "Millimeter-Wave High Radiation Efficiency Planar Waveguide Series-Fed Dielectric Resonator Antenna (DRA) Array: Analysis, Design, and Measurements," *IEEE Transactions on Antennas and Propagation,* vol. 59, no. 8, pp. 2834-2843, 2011.

[38] M. Ranjbar Nikkhah, J. Rashed-Mohassel and A. Kishk, "Compact Low-Cost Phased Array of Dielectric Resonator Antenna Using Parasitic Elements and Capacitor Loading," *IEEE Transactions on Antennas and Propagation,* vol. 61, no. 4, pp. 2318-2321, 2013.

[39] N. Larsen and O. Breinbjerg, "Analysis of Circularly Polarized Hemispheroidal Dielectric Resonator Antenna Phased Arrays Using the Method of Auxiliary Sources," *IEEE Transactions on Antennas and Propagation,* vol. 55, no. 8, pp. 2163-2173, 2007.

[40] O. Karabey, A. Mehmood, M. Ayluctarhan, H. Braun, M. Letz and R. Jakoby, "Liquid crystal based phased array antenna with improved beam scanning capability," *Electronic Letters,* vol. 50, no. 6, pp. 426-428, 2014.

[41] R. Kumari, K. Parmar and S. Behera, "A dual band triangular shaped DRA array for WLAN/WiMAX applications," in *India Conference (INDICON)*, Hyderabad, 2011.

[42] T. Elkarkraoui, N. Hakem and Y. Coulibaly, "DRA antenna with a superstrate at millimeter-wave," in *IEEE International Symposium on Antennas and Propagation* , Vancouver, BC, Canada, 2015.

[43] R. Tian, V. Plicanic, B. K. Lau and Z. Ying, "A Compact Six-Port Dielectric Resonator Antenna Array: MIMO Channel Measurements and Performance Analysis," *IEEE Transactions on Antennas and Propagation,* vol. 58, no. 4, pp. 1369-1379, 2010.

[44] J.-B. Yan and J. Bernhard, "Design of a MIMO Dielectric Resonator Antenna for LTE Femtocell Base Stations," *IEEE Transaction on Antennas and Propagation,* vol. 60, no. 2, pp. 438-444, 2012.

[45] L. Thamae and Z. Wu, "Dielectric resonator-based multiple-input multipleoutput antennas and channel characteristic analysis," *IET Microaves, Antennas and Propagation,* vol. 6, no. 9, pp. 1084-1089, 2012.

[46] J.-B. Yan and J. Bernhard, "Implementation of a Frequency-Agile MIMO Dielectric Resonator Antenna," *IEEE Transactions on Antennas and Propagation,* vol. 61, no. 7, pp. 3434-3441, 2013.

[47] Y. Zhang, A. Kishk, A. Yakovlev and A. Glisson, "Analysis of Wideband Dielectric Resonator Antenna Arrays for Waveguide-Based Spatial Power Combining," *IEEE Transactions on Microwave Theory and Techniques,* vol. 55, no. 6, pp. 1332-1340, 2007.

[48] K. Ishimiya, Z. Ying and J.-i. Takada, "A compact MIMO DRA for 802.11n application," in *IEEE Antennas and Propagation Society International Symposium*, San Diego, CA, 2008.

[49] K. Ishimiya, J. Langbacka, Z. Ying and J.-i. Takada, "A Compact MIMO DRA Antenna," in *International Workshop on Antenna Technology: Small Antennas and Novel Metamaterials, 2008. iWAT 2008*, Chiba, 286 - 289.

[50] J. Nasir, M. Jamaluddin, M. Khalily, M. Kamarudin, Irfanullah and N. Nor, "A dual-port MIMO DRA with high isolation for LTE application," in *IEEE Asia-Pacific Conference on Applied Electromagnetics (APACE)*, Johor Bahru , 2014.

[51] I. Shoaib, Y. Gao, K. Ishimiya, X. Chen and Z. Ying, "Performance evaluation of the 802.11n Compact MIMO DRA in an indoor environment," in *3rd European Conference on Antennas and Propagation (EuCAP)*, Berlin, 2009.

[52] Y. Li, I. Shoaib, S. Wang, X. Chen and Z. Ying, "A pattern reconfigurable DRA array for MIMO applications," in *IEEE International Conference on Microwave Technology & Computational Electromagnetics (ICMTCE)*, Beijing , 2011.

VITAE

Name : Mohamed Tammam Hussein

Nationality : Egyptian

Date of Birth : 8/19/1989

Email : mohammed.t.hussein@gmail.com

Address : Khobar, Saudi Arabia

Academic Background : Bachelor of Science in Applied Electrical Engineering, King Fahd University of Petroleum and Minerals

Publications

M.T. Hussain, O. Hammi, M.S. Sharawi, S.K. Podilchak, Y.M.M Antar, "A dielectric resonator based millimeter-wave MIMO antenna array for hand-held devices“ *IEEE International Symposium on Antennas and Propagation & USNC/URSI National Radio Science Meeting*, pp.3-4, 2015.

M.T. Hussain, M.S. Sharawi, S.K. Podilchak, Y.M.M Antar, "Closely Packed mm-Wave MIMO Antenna Arrays with Dielectric Resonator Elements” *10th European Conference on Antennas and Propagation, to be held in Davos, Switzerland*, on 10-15 April 2016. (Accepted).